EXPLORING THE EFFECT OF CLIMATE PERTURBATIONS ON WATER VAILABILITY FOR RENEWABLE ENERGY DEVELOPMENT IN THE INDIAN WELLS VALLEY, CALIFORNIA

by

David M. Rey

A Thesis submitted to the Faculty and Board of Trustees of the Colorado School of Mines in partial fulfillment of the requirements for the degree of Masters of Science (Hydrology).

Golden, Colorado

Date:_____

Signed:_____

David M Rey

Signed:_____

Dr. Kamini Singha

Thesis Advisor

Golden, Colorado

Date:_____

Signed:_____

Dr. Terri Hogue

Director

Hydrologic Science and Engineering

ABSTRACT

Energy and water are connected through the water-use cycle (e.g. obtaining, transporting, and treating water) and thermoelectric energy generation, which converts heat to electricity via steam-driven turbines. As the United States implements more renewable energy technologies, quantifying the relationships between energy, water, and land-surface impacts of these implementations will provide policy makers the strengths and weaknesses of different renewable energy options. In this study, a MODFLOW model of the Indian Wells Valley (IWV), in California, was developed to capture the water, energy, and land-surface impacts of potential proposed 1) solar, 2) wind, and 3) biofuel implementations. The model was calibrated to pre-existing groundwater head data from 1985 to present to develop a baseline model before running two-year predictive scenarios for photovoltaic (PV), concentrating solar power (CSP), wind, and biofuel implementations. Additionally, the baseline model was perturbed by decreasing mountain front recharge values by 5%, 10%, and 15%, simulating potential future system perturbations under a changing climate. These potential future conditions were used to re-run each implementation scenario. Implementation scenarios were developed based on population, typical energy use per person, existing land-use and land-cover type within the IWV, and previously published values for water use, surface-area use, and energy-generation potential for each renewable fuel type. The results indicate that the quantity of water needed, localized drawdown from pumping water to meet implementation demands, and generation efficiency are strongly controlled by the fuel type, as well as the energy generating technology and thermoelectric technologies implemented. Specifically, PV and wind-turbine (WT) implementations required less than 1% of the estimated annual aquifer recharge, while technologies such as biofuels and CSP, which rely on thermoelectric generation, ranged from 3% to 20%. As modeled groundwater elevations declined in the IWV, the net generation (i.e. energy produced – energy used) of each renewable energy implementation decreased due a higher energy cost for pumping groundwater. The loss in efficiency was minimal for PV and wind solutions, with maximum changes in the drawdown being less than 10 m; however, for CSP and biofuel implementations drawdowns over 50 m were observed at the pumping well, resulting in electrical generation efficiency losses between 4% and 50% over a two-year period. It was concluded that PV would be the best balance between water and land-use for the IWV, or other groundwater dependent Basin and Range settings. In areas with limited water resources but abundant available land for

implementation, WT solutions would have the smallest hydrologic impact. The impact of renewable scenarios was highly variable across and within differing fuel types, with the potential for larger negative impacts under a changing climate in areas with no perennial surface water.

TABLE OF CONTENTS

ABSTRACT……...iii

LIST OF FIGURES AND TABLES……..vi

ACKNOWLEDGEMENTS……...vii

CHAPTER 1 GENERAL INTRODUCTION……1

CHAPTER 2 EXPLORING THE EFFECT OF CLIMATE PERTERBATIONS ON WATER AVALIABILITY FOR RENEWABLE ENERGY DEVELOPMENT IN THE INDIAN WELLS VALLEY, CALIFORNIA……..……3

2.1 Abstract……3

2.2 Introduction……..4

2.3 Background……..7

2.3.1 Impacts of climate change on groundwater……7

2.3.2 The role of renewable energy generation in the energy-water nexus……..8

2.3.3 Renewable energy and cooling technologies……...8

2.3.4 Location and Climate……...9

2.3.5 Hydrogeology……12

2.4 Model development and parameterization……13

2.4.1 Model grid and layer design……..14

2.4.2 Boundary conditions and hydrologic flux development……17

2.4.3 Model calibration……...18

2.4.4 Future scenario development……21

2.5 Results……24

2.6 Conclusions……31

REFERENCES……..33

APPENDIX A……36

LIST OF FIGURES AND TABLES

Figure 1.1 General location of the Indian Wells Valley, CA……1

Figure 2.1 General location of the Indian Wells Valley, CA……..11

Figure 2.2 30 year average annual and monthly precipitation values derived from PRISM climate group data……13

Figure 2.3 15 year average annual and monthly evapotranspiration values derived from SSEBOP data……14

Figure 2.4 Resistivity and lithology log example from the Indian Wells Valley……17

Figure 2.5 Lithology distribution used to populate Sequential Indicator Simulation Algorithm……...18

Figure 2.6 Groundwater model grid and boundaries……...19

Figure 2.7 Difference between the PRISM precipitation and SSEBOP evapotranspiration data sets……...20

Figure 2.8 Groundwater model calibration data availability and distribution……21

Figure 2.9 Observed vs. Simulated groundwater elevations……..22

Figure 2.10 Mean absolute and root mean square error of model residuals for each calibration effort……23

Figure 2.11 Area map of model residuals……24

Figure 2.12 Time-series of observed vs. modeled groundwater elevation for three wells in the model domain……...25

Figure 2.13 Land cover and land use data for the Indian Wells Valley……....26

Figure 2.14 Water and land use required to meet energy demands for a variety of renewable energy technologies……...…27

Figure 2.15 Drawdown curves for each model simulation and renewable technology type……28

Figure 2.16 Energy required to pump groundwater needed for renewable energy technologies……...29

Figure 2.17 Water used by each technology compared to total water use within the basin……...30

Figure 2.18 Water used by each technology compared to total recharge within the basin……...31

Table 2.1 Indian Wells Valley population and calculated electricity usage for 2010 to 2015……...26

ACKNOWLEDGEMENTS

I would like to thank my Committee for the invaluable assistance and feedback over the duration of the project. Specifically, Kamini Singha for her continued time and efforts helping this project come together. Additionally I would like to thank members of my research group, Ryan Harmon, and Emily Voytek for their feedback and suggestions during the duration of the project.

CHAPTER 1

GENERAL INTRODUCTION

Earth is commonly referred to as the "Blue Planet", and while the majority of the earth's surface is covered by water, only 2.5% of that water is freshwater [*Stillwell et al.*, 2011]. Considering the growth rates in global population, this small amount of available freshwater will need to sustain an increasing number of communities [*Tanaka et al.*, 2006; *Famiglietti et al.*, 2011]. Unfortunately, earth's freshwater resources are not evenly distributed, and a large percentage of

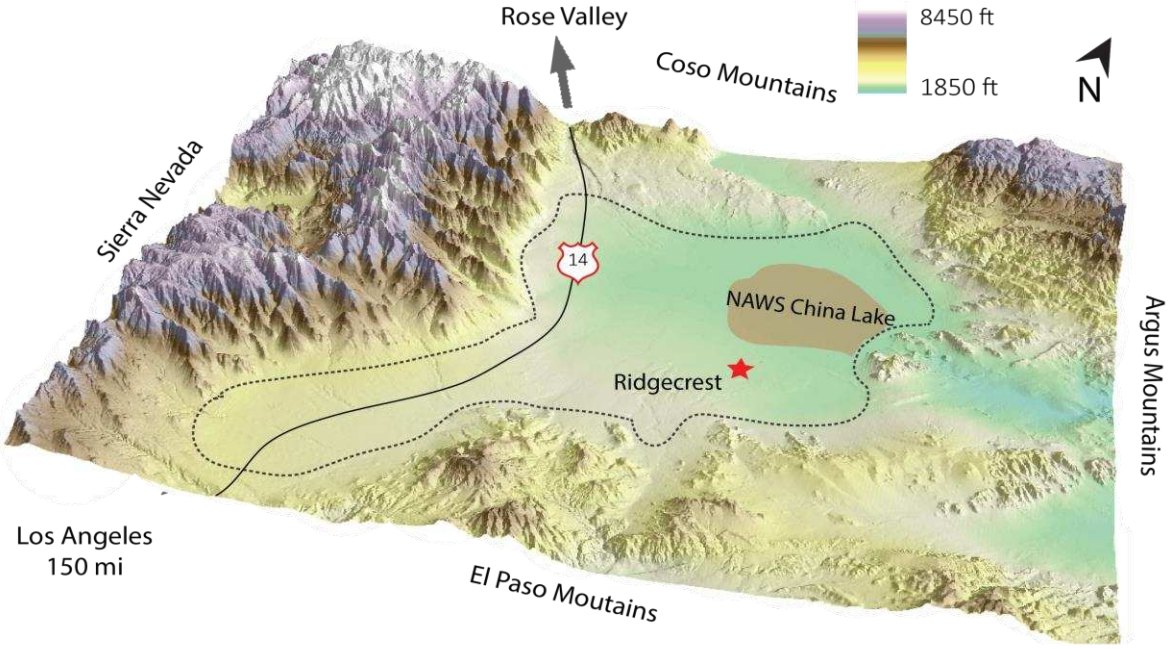

Figure 1.1 – The IWV, pictured above, is a topographic depression bounded by the Sierra Nevada, Coso, Argus, and El Paso mountain ranges which are the primary source of recharge for the IWV aquifer. The dotted line indicates the rough extent of the alluvial aquifer, and the numerical model used here.

population growth, particularly in the United States, is occurring in semi-arid and arid environments [*MacDonald*, 2010]. This growth has increased the demand for both water and energy, highlighting the importance of water and energy resources in regions where many communities are already reliant on groundwater as a primary source of potable water. Balancing regional energy and water demands in areas experiencing population growth requires the two

resources be managed in concert. The coupled dependence of energy production on water and water production on energy has been coined “The Energy-Water Nexus”.

At the state and federal levels, attempts to manage energy and water simultaneously are resulting in policies promoting water sustainability, energy-use reduction, and greenhouse-gas mitigation. These policies include increased investment in and the deployment of renewable energy solutions to meet growing energy demands. However, the implementation of renewable energy projects is clustered, depending on the availability of fuels such as solar, wind, or biomass. Many Basin and Range settings in the southwestern United States experience high quantities of incoming solar radiation, and a large number of windy days, creating favorable conditions for solar and wind implementations. Additionally, the availability of open land and the reliance of local economies on energy and water for food production strengthen the argument for renewable energy implementation within the region. However, increasing populations, high dependence on groundwater, and uncertainty associated with water availability under a changing climate make the feasibility and impact of some renewable solutions within the region unclear.

To assess the feasibility and hydrologic impact of potential renewable energy implementations, we quantified the land use and water use required for a variety of renewable energy types to meet energy demands in the Indian Wells Valley (IWV) of California’s Central Valley. I compared common renewable energy types and their impact on the IWV’s hydrologic cycle. Three fuel sources—solar, wind and biomass—and four energy generating technologies—photovoltaics (PV), wind-turbines (WT), concentrating solar power (CSP), and biomass power plants (BPP)—were considered. Two of these energy generating technologies (i.e. PV, WT) turn their primary fuel source directly into electricity. The other two energy generating technologies (i.e. CSP and biomass) rely on heating a fluid with energy harnessed from the sun or combustion of biomass to power steam-driven turbines. This process is called thermoelectric generation and has a variety of thermoelectric technologies associated with cooling and circulation of the heated fluid. Water is commonly used as the fluid in thermoelectric generation, making energy generating technologies leveraging thermoelectric generation more water intensive.

A numerical model was created of the IWV aquifer to test the impact of predicted human-induced groundwater change for energy development as a function of renewable energy type and potential hydrologic conditions under a changing climate. Specifically, electrical demand for the IWV was calculated based on the local population, and was used to evaluate the

size of each renewable scenario needed in terms of both land-footprint and water use. By leveraging a MODFLOW groundwater model of the IWV calibrated to historical data, we ran future scenarios to simulate pumping over the span of two years to assess initial aquifer responses to each renewable implementation scenario. Additionally, the amount of water recharging the IWV aquifer from the surrounding mountain ranges was changed to reflect potential decreases in aquifer recharge under a changing climate. Since there is no surface water available for use in the IWV, the energy cost associated with pumping groundwater locally was calculated for each scenario.

The hydrologic impact of each scenario was based on the total water used as a percentage of incoming precipitation and the drawdown at pumping wells used to supply water demands. Model results indicated that the hydrologic impact of renewable energy generation was highly variable when different fuel types were compared, and when different energy generating or thermoelectric technologies within the same fuel type (i.e. PV vs. CSP) were compared. Specifically, when results were organized by the cooling or circulation technology type used in the thermoelectric generation process (e.g. thermoelectric generation not used, dry-cooled, wet-cooled, etc.) as opposed to fuel type, the hydrologic impact of renewable energy generation was less variable. Consequently, the impact of renewable energy generation on the IWV aquifer is highly dependent on the energy generating technology as well as the cooling and circulation technology (i.e. if thermoelectric generation is used) deployed, not just the fuel type used. When the amount of water available to the model was decreased (i.e. by 5%, 10%, and 15%) to simulate a changing climate, the groundwater table unsurprisingly dropped. This change in groundwater elevation required more energy to be used to withdraw the water needed to run each renewable scenario. Consequently, if groundwater elevations in the IWV continue to decline, renewable energy implementations will continue to decrease in efficiency. Groundwater modeling plays an important role in evaluating the optimal location and long-term feasibility of renewable energy implementation scenarios.

CHAPTER 2
EXPLORING THE EFFECT OF CLIMATE PERTURBATIONS ON WATER AVAILABILITY FOR RENEWABLE ENERGY DEVELOPMENT IN THE INDIAN WELLS VALLEY, CALIFORNIA

A paper to be submitted to *Journal of Hydrology: Regional Studies*

David M. Rey[1], Kamini Singha[2]

2.1 Abstract

Energy and water are connected through the water-use cycle (e.g. obtaining, transporting, and treating water) and thermoelectric energy generation, which converts heat to electricity via steam-driven turbines. As the United States implements more renewable energy technologies, quantifying the relationships between energy, water, and land-surface impacts of these implementations will provide policy makers the strengths and weaknesses of different renewable energy options. In this study, a MODFLOW model of the Indian Wells Valley (IWV), in California, was developed to capture the water, energy, and land-surface impacts of potential proposed 1) solar, 2) wind, and 3) biofuel implementations. The model was calibrated to pre-existing groundwater head data from 1985 to present to develop a baseline model before running two-year predictive scenarios for photovoltaic (PV), concentrating solar power (CSP), wind, and biofuel implementations. Additionally, the baseline model was perturbed by decreasing mountain front recharge values by 5%, 10%, and 15%, simulating potential future system perturbations under a changing climate. These potential future conditions were used to re-run each implementation scenario. Implementation scenarios were developed based on population, typical energy use per person, existing land-use and land-cover type within the IWV, and previously published values for water use, surface-area use, and energy-generation potential for each renewable fuel type. The results indicate that the quantity of water needed, localized drawdown from pumping water to meet implementation demands, and generation efficiency are strongly controlled by the fuel type, as well as the energy generating technology and thermoelectric technologies implemented. Specifically, PV and wind-turbine (WT) implementations required

[1] Graduate student and primary researcher, Colorado School of Mines, Golden, CO 80401, USA
[2] Professor, Colorado School of Mines, Golden, CO 80401, USA

less than 1% of the estimated annual aquifer recharge, while technologies such as biofuels and CSP, which rely on thermoelectric generation, ranged from 3% to 20%. As modeled groundwater elevations declined in the IWV, the net generation (i.e. energy produced – energy used) of each renewable energy implementation decreased due a higher energy cost for pumping groundwater. The loss in efficiency was minimal for PV and wind solutions, with maximum changes in the drawdown being less than 10 m; however, for CSP and biofuel implementations drawdowns over 50 m were observed at the pumping well, resulting in electrical generation efficiency losses between 4% and 50% over a two-year period. It was concluded that PV would be the best balance between water and land-use for the IWV, or other groundwater dependent Basin and Range settings. In areas with limited water resources but abundant available land for implementation, WT solutions would have the smallest hydrologic impact. The impact of renewable scenarios was highly variable across and within differing fuel types, with the potential for larger negative impacts under a changing climate in areas with no perennial surface water.

2.2 Introduction

Quantifying the 1) energy costs of water infrastructure and the 2) water costs of energy infrastructure are required to balance future energy portfolios with regional water demands [*Bazilian et al.*, 2011]. Currently, 40% of domestic energy produced from primary sources (e.g. coal, petroleum, natural gas, nuclear power, and renewable energy) is used to generate electricity [*U.S. EIA*, 2016]. 89% of electricity produced comes from thermoelectric power plants that convert heat to electricity [*Macknick et al.*, 2012a; *Healy et al.*, 2015]. The conversion process uses a primary energy source to power steam-driven turbines. Converting water to steam accounts for 45% of all domestic freshwater withdrawals [*Healy et al.*, 2015], making thermoelectric generation the single largest source of freshwater withdrawals in the United States [*Maupin et al.*, 2014]. Similarly, water use is an energy-intensive process; water extraction, treatment, distribution, and wastewater processing all have significant energy needs. For example, estimates of energy use for water treatment and transport in California are as high as 20% of the state's total electrical generation [*CEC 2005*].

Several factors complicate balancing water and energy budgets. Specifically, the non-uniform distribution of domestic energy production, water availability, and population growth create regional hotspots that are more sensitive to the coupled nature of the energy-water nexus. For example, the southwestern United States is a water-stressed region with a growing

population and energy-water footprint. Recent population statistics estimate that by 2030, the southwestern United States will experience a population increase of 70% [*MacDonald*, 2010]. Simultaneously, the region has seen increased investment in, and deployment of, renewable-energy technologies to meet legislative mandates and mitigate greenhouse gas (GHG) emissions [*Lewis*, 2007; *Ong et al.*, 2013]. Pre-existing or recently identified areas for solar, wind, biofuels, and geothermal energy generation predominantly fall in Basin and Range settings within the southwestern United States due to the region's high rate of incoming solar radiation, geothermal activity, abundance of public open space, and higher than average percentage of windy days. The Basin and Range province contains basin-fill aquifers that often represent the exclusive source of water within the region, commonly resulting in overuse [*Leake and Konieczki*, 2000; *Famiglietti*, 2014]. Consequently, the hydrologic footprint of potential renewable energy implementations in the southwestern Basin and Range (SWBR) is integral to the region's future energy and water security, which is a growing concern as population increases and the climate warms [*MacDonald*, 2010].

Further contributing to complexity of the energy-water nexus within the SWBR is the uncertainty associated with the effect of climate perturbations on regional water availability. As increasing GHG concentrations influence climate variables such as temperature and precipitation, there is a direct influence on groundwater resources, including perturbations in aquifer-recharge mechanisms due to changes in evapotranspiration (ET), precipitation, and infiltration [*Taylor et al.*, 2013]. Within the SWBR, a significant component of recharge to basin-fill aquifers occurs along the mountain front [*Meixner et al.*, 2015](. Traditionally called mountain-front recharge (MFR), this process is the primary aquifer recharge mechanism in Basin and Range settings [*Wilson and Guan*, 2004]. For MFR-dominated regions such as the Sierra Nevada, climate change and the increasing likelihood of extreme climactic events will perturb two distinct hydrologic variables controlling aquifer recharge: (1) less precipitation will fall as snow due to increasing winter temperatures; and (2) a higher water fraction will be lost to ET as more energy becomes available [*Foster et al.*, 2016].

This study focuses on the feasibility of renewable energy generation in SWBR, which is a groundwater-dependent ecosystem, using the Indian Wells Valley (IWV) in California as a test case example. This study focuses on the IWV for several reasons: (1) a multitude of renewable-energy projects have been proposed in this basin as well as systems with similar geography,

particularly in California, which generates the most kWh of electricity from renewable sources ; (2) this system is reliant on groundwater resources, like other SWBR physiographic settings, making the exploration of the water-energy nexus important from a water-limitation perspective [*Maupin et al.*, 2014]; (3) the basin-fill aquifers underlying this region are among the most overused in the U.S. [*Leake and Konieczki*, 2000] and have experienced declining water tables resulting in land subsidence, and water quality degradation [*Thomas and Famiglietti*, 2014]; and (4) future climate and hydrologic projections have identified this part of the U.S. as having a high potential for hydrologic change [*Cook et al.*, 2004; *Seager et al.*, 2007; *Barnett et al.*, 2008]. Additionally the IWV has been identified by the California Department of Water Resources as being in "critical overdraft" (www.water.ca.gov/groundwater/sgm), which means that a continuation of the current water-use and management would potentially result in significant and adverse environmental, social, and economic impacts.

In this study, a MODFLOW model of the IWV was developed to conduct an assessment of groundwater impacts and net energy productivity under different solar, wind, and biomass implementation scenarios. Each scenario was run using a calibrated model with varying magnitudes of MFR (i.e. current recharge, 5% less, 10% less and 20% less) to capture future uncertainty in water quantity and generation efficiency associated with climate change. The model was calibrated to groundwater head data attained from Kern County Water Agency for the years from 1985 to present. The calibrated model was used to run predictive scenarios in which wind, photovoltaic (PV), concentrating solar power (CSP), and biofuel implementations were used to generate the power for the IWV. Scenarios were developed based on population, typical energy use per person, existing land-use and land-cover type within the IWV, and previously published values for water use, surface-area use, and energy-generation potential for each renewable energy fuel type. By establishing a baseline, calibrated model to represent current conditions, we simulated pumping based on the water required for the desired magnitude of energy generation for each renewable implementation scenario. Implementation scenarios were developed based on the average energy use per person within the region, the water required to generate this amount of electricity for each renewable type, and the land-footprint required to meet the IWV's energy demand. Water was pumped from regions in the IWV with a large enough area to support the land footprint of each scenario, and a suitable land-use and land-cover type for a renewable energy implementation. This approach allowed us to analyze the

relationships between energy, water, and land-area needed for each renewable energy fuel type, and how implementation efficiency may be altered under a changing climate.

2.3 Background

2.3.1. Impacts of climate change on groundwater

Climate change impacts groundwater resources by perturbing aspects of the hydrologic cycle related to air temperatures, weather patterns, and land-surface evaporation [*Vorosmarty et al.*, 2000; *Barnett et al.*, 2008; *Luce et al.*, 2013]. Specifically: (1) changes in sea surface temperatures affect patterns in terrestrial precipitation and extreme weather events [*Dai*, 2013]; (2) increasing terrestrial air temperatures decrease the fraction of precipitation falling as snow, altering the seasonal hydrograph [*Godsey et al.*, 2014]; (3) higher energy availability increases terrestrial ET rates, decreasing the fraction of precipitation infiltrating into aquifers [*Cook et al.*, 2014b; *Seager et al.*, 2015; *Williams et al.*, 2015]; and (4) decreases in surface water availability will increase the reliance of many communities on groundwater resources.

Increasing global air temperatures are driving changes in sea surface temperatures, altering precipitation patterns, and increasing the probability of extreme climactic events. A relevant example is the 2012-2014 California drought, which has been attributed to a persistent atmospheric high-pressure region responsible for altering the typical trajectory of the California winter storm track northward [*Seager and Hoerling*, 2014; *Wang et al.*, 2014; *Seager et al.*, 2015]. This region of high pressure, called "The Ridiculously Resilient Ridge", resulted in a multi-year drought event characterized as one of the most severe in the instrumental record [*Robeson*, 2015]. The high-pressure anomaly was the result of multiple factors, including atmospheric variability, [*Seager and Hoerling*, 2014; *Seager et al.*, 2015; *Swain*, 2015], warming in both tropical and mid-latitude sea surface temperatures [*Wang et al.*, 2014; *Hartmann*, 2015; *Swain*, 2015], and anthropogenic contributions to climate change [*Cook et al.*, 2014a; *Seager and Hoerling*, 2014; *Williams et al.*, 2015].

In general, increasing mean global temperatures are altering the intensity, duration, frequency, and form of seasonal precipitation as warmer winter temperatures are increasing [*Stewart et al.*, 2005; *Cayan et al.*, 2007; *Barnett et al.*, 2008; *Trenberth*, 2011]. The result has been observed decreases in snow accumulation [*Brown and Robinson*, 2011], which is a vital component for sustaining summer base flows in rivers [*Tague et al.*, 2008; *Godsey et al.*, 2014; *Markovich et al.*, 2016] and recharging aquifers in snow-dominated regions [*Meixner et al.*, 2015]. The

presence of mountain snow acts as a natural reservoir, and changes in its seasonal distribution are linked to land-surface feedbacks affecting the partitioning of soil moisture, and its infiltration into groundwater systems [*Bales et al.*, 2006].

Increased terrestrial surface temperatures are additionally driving higher rates of ET [*Brutsaert*, 2006] leading to decreases in terrestrial soil moisture [*Trenberth*, 2011], exacerbating the hydrologic impacts of periods with lower-than-average precipitation [*Robeson*, 2015; *Swain*, 2015], and altering the partitioning of available water in the terrestrial water balance. Additionally, increasing land-surface temperatures may increase the probabilities of "hot droughts" in which both abnormally high temperature and abnormally low precipitation occur simultaneously [*AghaKouchak et al.*, 2014; *Hao et al.*, 2014; *Leonard et al.*, 2014]. The abnormally high temperatures associated with the recent California drought increased the severity of the drought when compared with other time periods experiencing similar rates of decreased precipitation [*AghaKouchak et al.*, 2014; *Griffin and Anchukaitis*, 2014; *Shukla et al.*, 2015; *Swain*, 2015; *Williams et al.*, 2015].

Despite recent research, the timing and magnitude of predicted hydrologic and climactic changes remains uncertain [*Sherwood and Fu*, 2014]. Ambiguity exists surrounding future concentrations of GHGs in the atmosphere and the effect these concentrations will have on variables that drive MFR such as land-surface temperature and precipitation. Additionally, the degree to which population, drought, and regulation will influence future groundwater withdrawals is difficult to predict.

2.3.2. The role of renewable energy generation in the energy-water nexus

Renewable energy solutions have the ability to provide electric power with a smaller water footprint than many other conventional generation methods, facilitating the balance between energy and water use. However, decreased hydropower efficiency associated with lower streamflows [*Christensen et al.*, 2004], the halt of thermoelectric power plants in times of drought [*Macknick et al.*, 2012a], and increasing energy demands are reinforcing the need for balanced water use and energy use. In 2012, the Department of Interior created a plan to implement less water-intensive electrical generation on public land within the southwestern United States, which has helped drive a majority of the implemented, or proposed renewable energy solutions in the region [*BLM*, 2012]. To date, the BLM has approved 34 utility-scale renewable energy projects in SWBR settings. While renewable energy resources have a lower

water footprint than conventional electrical generation techniques, their implementation is still limited by the availability of a fuel source (e.g. solar, wind), but also by water and land-availability [*Macknick et al.*, 2012b; *Ong et al.*, 2013]. These impacts have driven previous research to help quantify water demands associated with different renewable energy fuel types, as well as the ties between generation capacity (i.e. how much electricity can be generated) and land-use [*Bazilian et al.*, 2011]. Specifically, work relating to the water use [*Macknick et al.*, 2012a, 2012b] and land-use impacts [*Ong et al.*, 2013] of renewable energy resources has provided a range of estimated values for both water and land use for each renewable fuel type; these estimates have been used by others to calculate the hydrologic demand of different renewable energy implementation scenarios across the country. However, these studies estimated hydrologic impacts from the perspective of total regional water use, failing to simulate the hydrologic impact of renewable energy generation on groundwater resources in regions with minimal perennial surface water.

2.3.3. Renewable energy and cooling technologies

The most common renewable energy fuel types to be considered in the SWBR are solar, wind, and biomass-powered implementations. Each of these fuel types have sub-categories associated with different methods for turning the primary energy source (i.e. wind, solar, or biomass) into electricity. Specifically, each energy fuel source has associated energy generating technologies, and some energy generating technologies. For example, solar-powered generation can be divided into two energy generating technology categories: PV and CSP. PV solutions turn solar power directly into electricity, where CSP solutions use a more conventional thermoelectric process to generate electricity. Energy generating technologies requiring thermoelectric generation (e.g., CSP, biofuel) often use water as the working fluid (and as the cooling medium to condense steam) that drives the steam engine to generate electricity, and can employ a variety of cooling and circulation technologies. CSP facilities use water for steam cycle processes, for cleaning mirrors or heliostats, and for cooling if a cooling tower is used. PV systems require occasional panel washing. Biofuel facilities use water for cooling and for steam cycle processing. Wind systems require very little water, if any, for cleaning. PV and wind implementations do not rely on thermoelectric generation processes, whereas CSP and biomass implementations do. Different cooling system technologies used in the thermoelectric process for CSP and biomass implementations were considered in the work here by modeling their water demand. The cooling

systems used in model scenarios included wet recirculating technologies (evaporative cooling towers), once-through cooling systems (open loop cooling), air-cooled condensing (dry cooling), and hybrid wet and dry cooling systems (hybrid cooling) cooling systems. It should be noted that technologies utilizing thermoelectric generation (i.e. CSP, biofuels) have the capacity to store energy in the form of heat, meaning that generated energy is not lost immediately if there is no electrical demand. This is in direct opposition to technologies such as PV or wind that lose the generated electricity if it is not stored or used when generated.

2.3.4 Location and Climate

The IWV is located 200 km northeast of Los Angeles in the rain shadow of the Sierra Nevada mountain range, a semi-arid Basin-and-Range setting (Figure 2). The IWV is a topographic depression of roughly 750 km^2 and is bounded by the Sierra Nevada Mountains to the west, the Coso Range to the north, the Argus Range to the east, and the El Paso Mountains to the south [Figure 2, *Kunkel and Chase*, 1969]. The valley floor between these ranges lies at

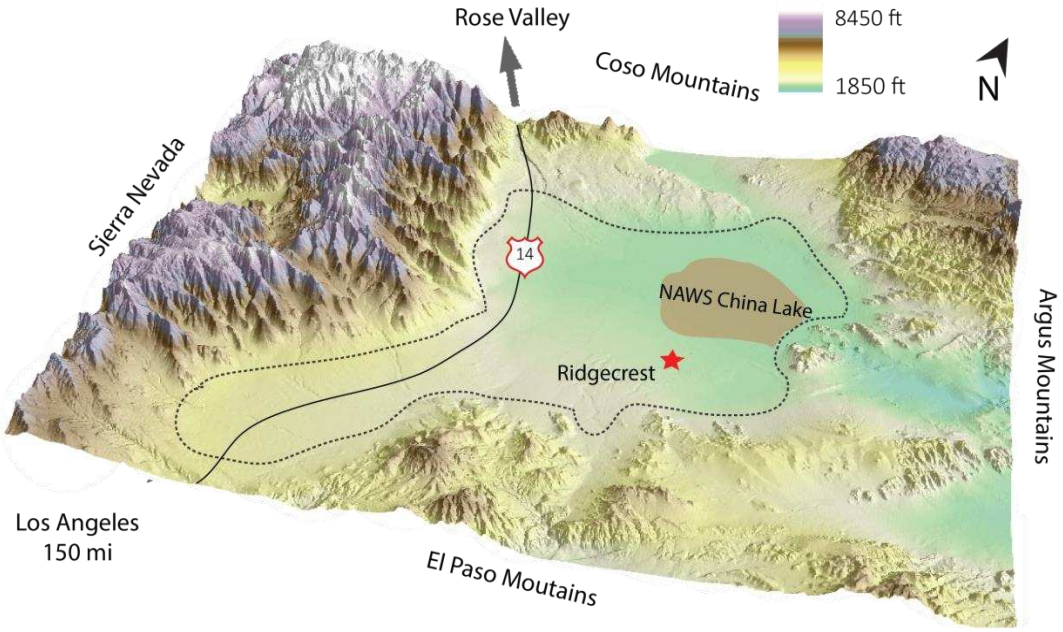

Figure 2.1 – The IWV, pictured above, is a topographic depression bounded by the Sierra Nevada, Coso, Argus, and El Paso mountain ranges which are the primary source of recharge for the IWV aquifer. The dotted line indicates the rough extent of the alluvial aquifer, and the numerical model used here.

elevations between 570 and 730 meters above sea level [*Berenbrock and Martin*, 1991]. Two major population centers exist within the IWV: (1) Ridgecrest, with a population of roughly

29,000; and (2) Inyokern, with a population of 1,000. Given the lack of perennial surface water within the basin, groundwater sustains the IWV's needs for agricultural, industrial, and domestic water supplies [*Moyle and Dutcher*, 1973; *Thyne*, 2004].

The IWV is a closed basin. Several studies in the past have suggested it is an open basin [*Thompson*, 1929; *Austin et al.,* 1988; *Thyne*, 2004]; however, this hypothesis has been discredited due to continually falling water table elevations despite pumping rates within the basin being substantially less than the recharge values proposed by the open basin hypothesis. Consequently the majority of studies within the region have treated the IWV as a closed basin [*Kunkel and Chase*, 1969; *Bloyd and Robson*, 1971; *Moyle and Dutcher*, 1973; *Berenbrock and Martin*, 1991; *Monastero*, 2002].

Precipitation within the IWV experiences distinct seasonal variations and is highly dependent on elevation (Figure 3). Due to the lack of adjacent weather stations at elevations above the valley floor, the Parameter-elevation Relationships on Independent Slopes Model (PRISM) dataset was used to estimate precipitation for this work. The PRISM data set is derived from a regression between climate and elevation for each existing gridcell; derived regressions incorporate existing climate and precipitation stations, which are subsequently weighted based on physiographic similarity with adjacent gridcells [*Daly et al.*, 2008]. The most important factors incorporated from existing climate and precipitation stations include: (1) location, (2) elevation, (3) slope orientation, (4) vertical atmospheric layering, and (5) orographic effectiveness of the local terrain [*Daly et al.*, 1994]. The PRISM dataset has compared favorably to other gridded precipitation products [*Daly et al.*, 1994, 2002; *Di Luzio et al.*, 2008], specifically in mountainous and coastal areas of the western United States, which are characterized by sparse data coverage, large elevation gradients, rain shadows, inversions, cold air drainage, and coastal effects.

November to March is the wet season, while the months of April to October are comparatively drier in both the valley floor and the surrounding mountains. At the valley floor, the IWV has a semi-arid climate that experiences annual rainfall totals between 100 to 150 mm of precipitation per year (Figure 3). All precipitation that falls on the valley floor is lost to ET prior to having the ability to infiltrate into the aquifer [*Kunkel and Chase*, 1969; *Berenbrock and Martin*, 1991; *Thyne*, 2004]. However, the bounding mountain ranges have an annual precipitation total exceeding 400 mm at elevations along the watershed boundary, mostly as

snow during the winter. As a result of the stark precipitation contrast with elevation, a majority of aquifer recharge occurs as MFR along the western portion of the basin [*Thyne*, 2004]. However, a small portion of MFR occurs along the basin-fill bedrock boundary with the Coso Mountains to the north, and the El Paso Mountains to the south.

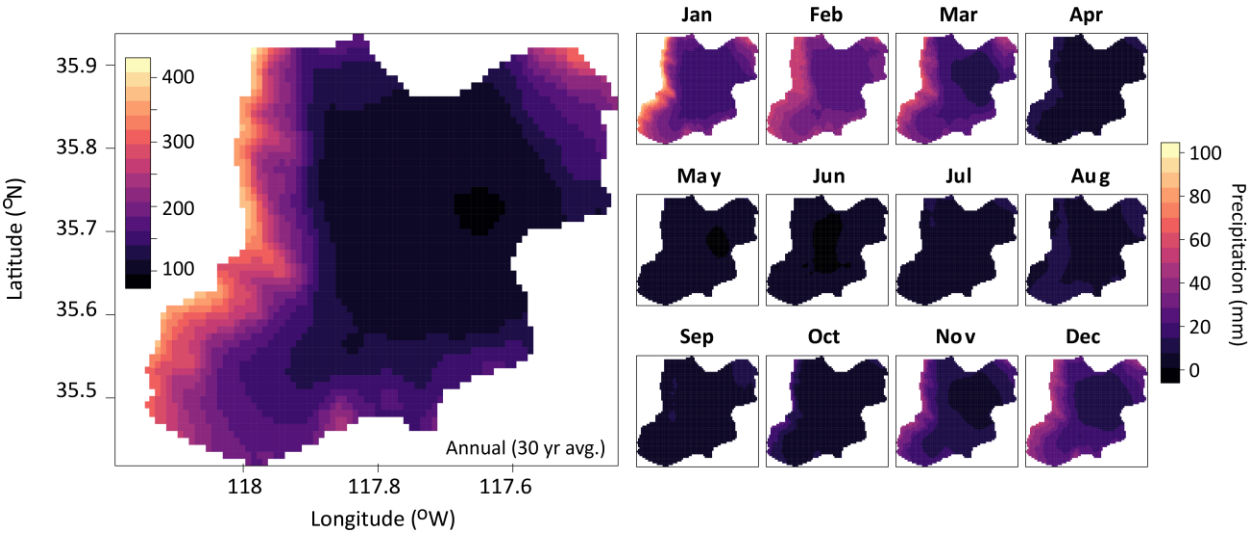

Figure 2.2 – 30-year average precipitation values of the conterminous United States were retrieved as a gridded precipitation product at 800 m^2 resolution from the PRISM Climate group website [http://prism.oregonstate.edu, created 12 Dec 2016]. Annual values (left), and monthly values (right) are reported in mm. In both annual and monthly values, the strong influence of elevation on precipitation within the IWV is apparent. Additionally, the seasonal wet and dry seasons can be seen in the monthly data.

ET within the IWV is poorly constrained, particularly at higher elevations due to the lack of available instrumentation. A gridded data set for ET (SSEBop) was obtained to estimate ET rates within the watershed. SSEBop data are a thermal-based ET estimation product based off ET fractions from remotely sensed MODIS thermal imagery collected every 8 days [*Mu et al.*, 2013] and model-simulated weather fields [*Senay et al.*, 2013]. Specifically, ET was computed from 2000 to present for the conterminous U.S. using both MODIS and Global Data Assimilation System (GDAS) data. SSEBop uses established boundary conditions for the hot and cold reference pixels (i.e. reference pixels used to determine the assumed linear relationship between land-surface and air temperatures) so that ET can be calculated as a function of the land-surface temperature, which is populated from remotely sensed data and reference ET from global weather datasets using the Simplified Surface Energy Balance (SSEB) approach [*Senay et al.*,

2013; *Singh et al.*, 2013; *Velpuri et al.*, 2013]. When compared with eddy covariance data, SSEBop data explained 64% of the observed variability across diverse ecosystems in the conterminous U.S. during 2005 [*Senay et al.*, 2013]. Consequently, the SSEBop data were used as a starting point for the calibration of the hydrologic model as they were not expected to perfectly capture the actual ET within the IWV, especially over multiple years, given the complex mountainous terrain. The SSEBop data indicate ET rates at the valley floor ranging from 5 mm to 20 mm monthly (Figure 4). This matches previously published estimates that the majority of incoming precipitation that reaches the valley floor is lost to ET prior to infiltration. The Sierra Nevada mountains on the western edge of the watershed have the highest ET estimated values, predominantly as a function of receiving the largest amount of precipitation. The highest rates of ET occur during the warmer months of March to October, coinciding with the dry season, representing ET from accumulated snow in the Sierra Nevada mountain range. However, ET rates predicted by the SSEBop data set at the watershed boundaries are higher than precipitation values. Uncertainty in both of these datasets is discussed further in the sections below.

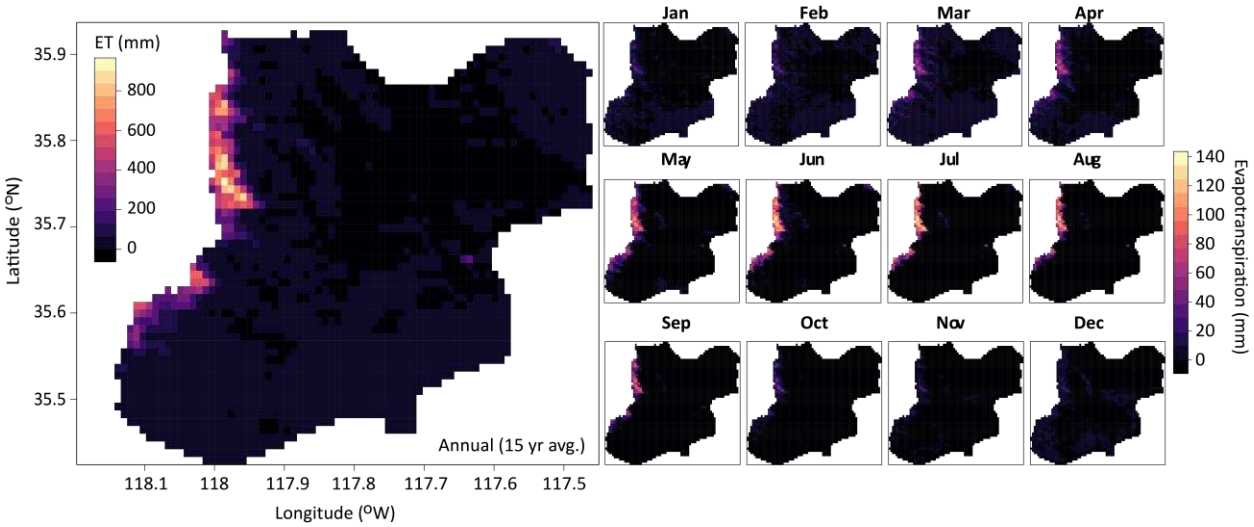

Figure 2.3 – Gridded precipitation data was obtained from the SSEBop dataset at the 1 km^2 resolution. These data were available from 2000 to 2015, and were averaged over the 15-year period to obtain average values across the watershed for ET. The largest ET values were over the Sierra Nevada mountains, a result of this area receiving the highest amount of precipitation. Additionally, months associated with the dry season have higher values of ET, partially due to the evapotranspiration from snow. Small values of higher ET can be seen on the east side of the basin, and coincide in location with the southern extent of the China Lake playa.

2.3.4 Hydrogeology

Unconsolidated basin-fill deposits within the valley extend to depths between 600 to 150 m deep from west to east, respectively [*Bloyd and Robson*, 1971]. These deposits are Tertiary continental deposits that consist primarily of gravel, sand, silt, and clay. The deposition of basin-fill deposits is primarily a function of: (1) previously existing alluvial fans entering the basin on the north, west, and south sides from the Coso, Sierra Nevada, and Argus mountain ranges; and (2) an ancestral lake which permitted the exchange of surface water and groundwater with the adjacent basins of the Rose Valley to the north and the Salt Valley to the south [*Berenbrock and Martin*, 1991]. Consequently, the basin-fill deposits comprising the IWV aquifer increase in percentage of fines from west to east.

Three major lithologic units help confine and control groundwater flow both vertically and laterally [*Monastero*, 2002]. These units include consolidated Quaternary and Tertiary volcanic rocks, Tertiary continental deposits, and pre-Tertiary basement complex [*Berenbrock and Martin*, 1991]. Quaternary and Tertiary volcanic rocks as well as pre-Tertiary basement complex confine groundwater flow [*Kunkel and Chase*, 1969]. The spatial distribution of Tertiary continental deposits defines the extent of basin-fill deposits and subsequently the spatial extent of the IWV aquifer [*Moyle and Dutcher*, 1973]. Unconsolidated basin-fill includes alluvium and lacustrine deposits with interbedded gravel and sand decreasing in the percentage of gravels and sands moving eastward [*Monastero*, 2002]. As previously noted, the IWV is thought to be a closed basin with minimal groundwater exchange with adjacent basins.

Under natural conditions, the exclusive influx of water into the basin occurred as MFR from the adjacent mountain ranges and was balanced by ET at the China Lake playa located in the eastern portion of the valley [*Thyne*, 2004]. As the population within the IWV grew, groundwater pumping was used to provide water for agricultural and domestic purposes. Since the start of pumping in the 1920s, the groundwater table within the IWV has been consistently declining. The result is a regional mass balance comprised of (1) MFR contributing water to the basin-fill aquifer; (2) groundwater pumping removing water from the aquifer; and (3) ET at China Lake playa removing water from the aquifer.

Exactly 216 wells were available with data obtained from the Kern County Water Agency; however, only 16 penetrated the majority of the basin fill deposits, and had well logs associated with their drilling. Consequently, 16 wells located predominantly in the west side of the basin

were used to determine lithological characteristics for the basin-fill deposits. The remaining wells were associated with groundwater elevation data, and were used for model calibration.

2.4 Model Development and Parameterization

Groundwater model boundaries were created by using the distribution of basin-fill sediments to delineate the spatial extent of the aquifer. These boundaries were obtained as a shape file from the California Statewide Groundwater Elevation Monitoring program (https://www.casgem.water.ca.gov). Model cells between the aquifer extent and watershed boundaries, explained below, were set as no-flow cells. The model was run as a saturated zone model since we were interested in the behavior of the IWV aquifer in response to renewable energy implementations under decreasing MFR scenarios. MFR values were perturbed manually to examine how the aquifer responded to positive and negative recharge trends under different implementation scenarios. Specific climactic forcing data were not included in the model. Sixteen borehole logs distributed throughout the basin contained four major lithologic units: gravel, coarse sand, medium sand, fine sand, silt, and clay; however, no hydraulic conductivity or specific yield values were available for any of the reported units. Consequently, each lithology was assigned a distinct hydraulic conductivity and specific yield value representative of the particular lithology based on a range of published values for each lithology. The 16 wells obtained from the Kern County Water Agency were used to determine a potential geostatistical distribution of lithologies within the basin. The flow model was populated with PRISM precipitation data, SSEBop monthly ET data, simulated hydraulic conductivity and specific yield values, and groundwater pumping data provided by the Kern County Water Agency. The model was subsequently calibrated to groundwater elevation data from 1985 through present, using the model-independent Parameter Estimation and Uncertainty Analysis (PEST). Hydraulic conductivity, recharge, and ET values were optimized simultaneously to best fit observed groundwater head values, and simulate current aquifer conditions. Calibrated model results were then used to populate initial head conditions for exploring future energy-implementation scenarios. Details on each step are outlined below.

2.4.1 Model Grid and Layer Design

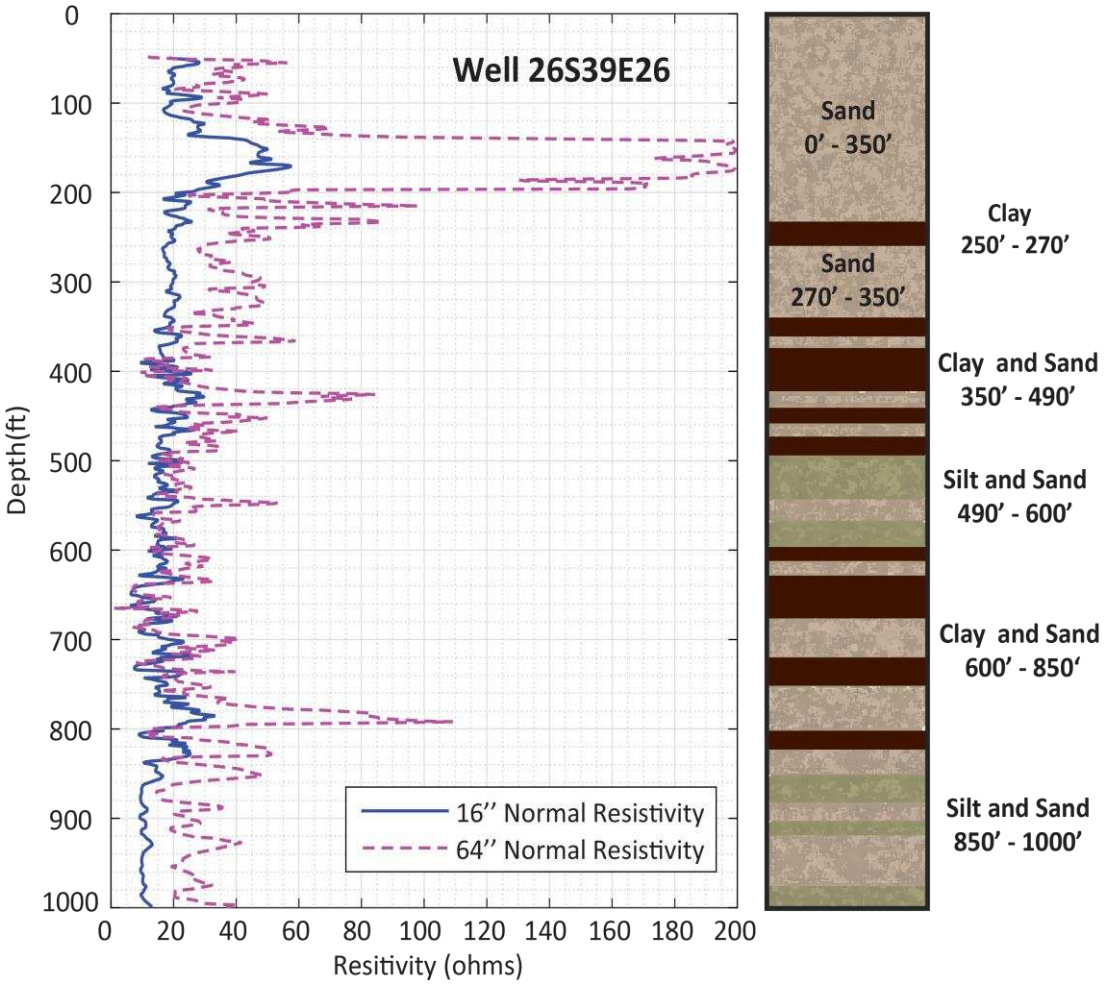

Figure 2.4 –Example of one of the 16 electric logs used to determine the potential lithologic distribution for the groundwater model. Separations in resistivity (i.e. 16" (41 cm) and 64" (163 cm) electrode spacing measurements) helped map permeable and porous units. Trends in these separations were compared with lithology logs, and in general, less separation in resistivity was observed at depths logged as clay and silt units.

ArcGIS was used to delineate the IWV watershed. First, a set of digital elevation maps (DEMs) that encompassed the IWV was obtained through the USGS National Elevation Dataset. The individual DEMs were mosaicked into a single DEM. This DEM was then preprocessed to eliminate artifact topographic depressions and flat regions using the ArcGIS fill tool. Once topographic artifacts were eliminated, the flow accumulation tool was used to delineate flow direction vectors based on the lowest point identified within the watershed. Finally, the watershed tool was used to extract a polygon of the IWV watershed. This polygon was then used as a mask to clip the DEM grid to the spatial extent of the watershed. The masked DEM of the watershed extent was used to determine the topography of the model's top layer.

Deeper layers were mapped from each of the 16 available wells. Each well contained electric logs of resistivity at different electrode spacings, to map lithology and capture the potential invasion of the drilling fluid, self potential, and lithology logs. Borehole logging systems provided 16 in (41 cm) "short" normal and 32 or 64 in (81 or 163 cm) "long" normal resistivity measurements. By utilizing multiple electrode spacings, it was possible to define zones of differing permeability and porosity. The well logs were digitized using Petra, and separations in resistivity for different electrode spacings were compared to lithology logs (Figure 5). This process was used to derive lithologies for each well for each vertical meter.

To gauge uncertainty stemming from lithologic heterogeneity within the IWV aquifer, multiple simulations of hydraulic conductivity fields were created using the Sequential Indicator Simulation (SISIM) package in Stanford Geostatistical Modeling Software (SGeMS) [*Remy et al.*, 2009]. SGeMS is an open-source tool for three-dimensional geostatistical modeling that has been used to simulate the spatial distribution of heterogeneous lithofacies [*Bianchi et al.*, 2009, [*Remy et al.*, 2009]]. Lithologies from the well logs were lumped into four categories including gravel with coarse sand, medium sand, fine sand, and silt with clay. Each lithology represents a distinct mutually exclusive hydraulic conductivity and specific yield category, and the combinations of the four lithologies represent an exhaustive distribution within the groundwater model.

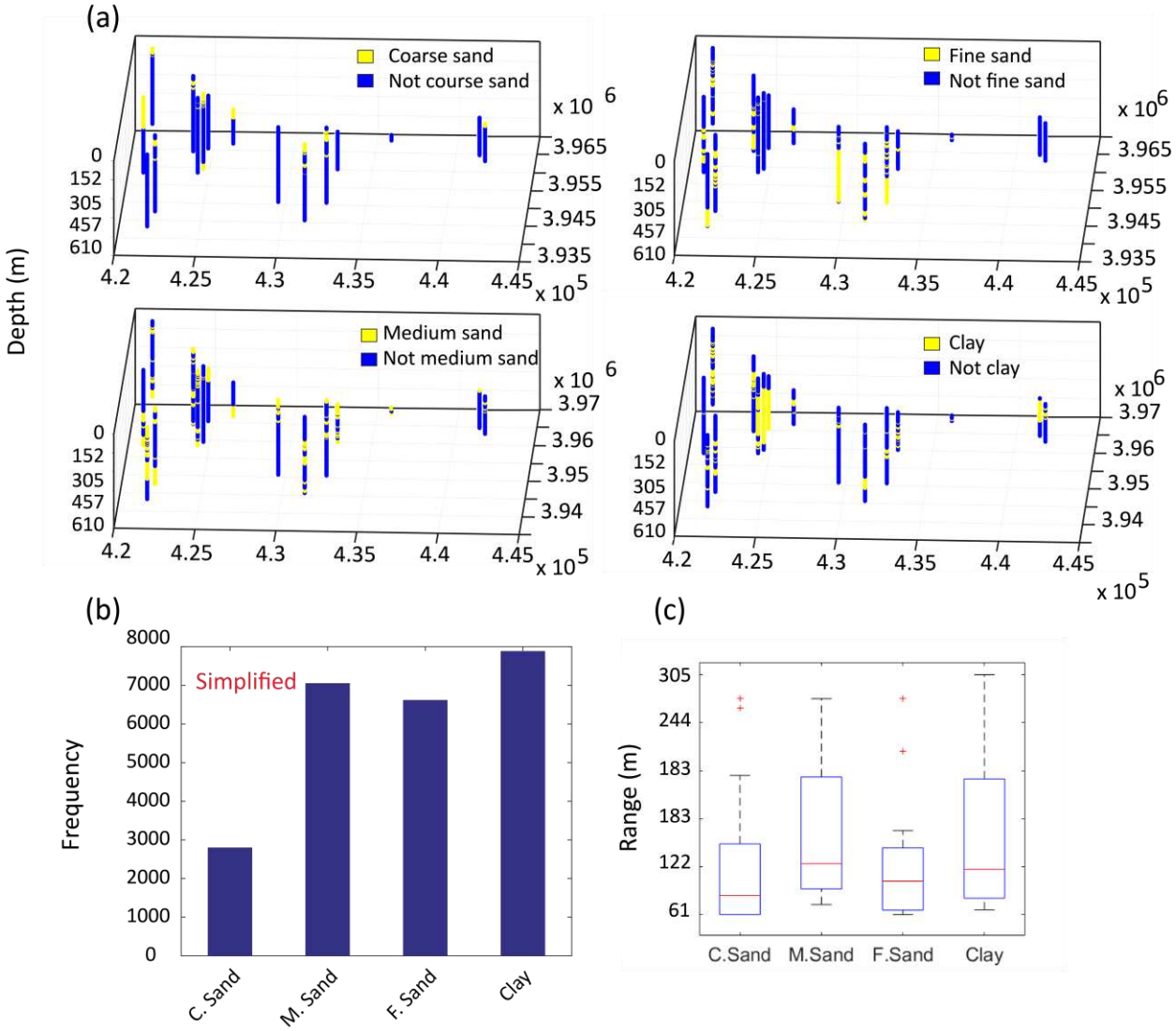

Figure 2.5 – (a) The 4 indicator distributions for coarse sand, medium sand, fine sand, and clay lithologies in the IWV for all well data available, (b) the relative combined distribution of each lithology in the 16 boreholes, (c) ranges of variograms fitted to each of the lithologies and used to derive model layer thicknesses, as well as parameterize rock property simulations.

Each lithology was treated as an indicator variable with a probability of one if the lithology is present, and a probability of zero if the lithology is not present. Marginal probabilities and experimental variograms were calculated for each indicator variable. Subsequently, the spatial relationships developed for each indicator variable were used to populate the SISIM algorithm to develop 35 equally probably lithologic distributions with four distinct hydraulic conductivity and specific yield values (Figure 6a). Thirty-five realizations were

chosen in an attempt to strike a balance between having a significant sample size of lithologic distributions, and computational efficiency.

Based on variogram modeling of the lithologies, mean vertical correlation lengths of ~60 m were observed for each lithology (Figure 6c). Based on estimates that the basin-fill deposit depths were roughly 600 meters thick, ten 60-m layers were created. It should be noted that empirical variograms derived and plotted in Figure 6c were fit to down-borehole data for each well and each lithology (i.e. 16 variograms for each lithology, 64 variograms in total). Well spacing did not enable reasonable variogram fits unless exclusively looking down-borehole; consequently it was assumed that lateral hydraulic conductivity was an order of magnitude larger than the range derived from down-hole variograms. Matlab was used to create a terrain-following grid from the elevation of the top layer. This process entailed subtracting the derived layer thickness from the model layer above to derive the height of each subsequent layer (Figure 2.6).

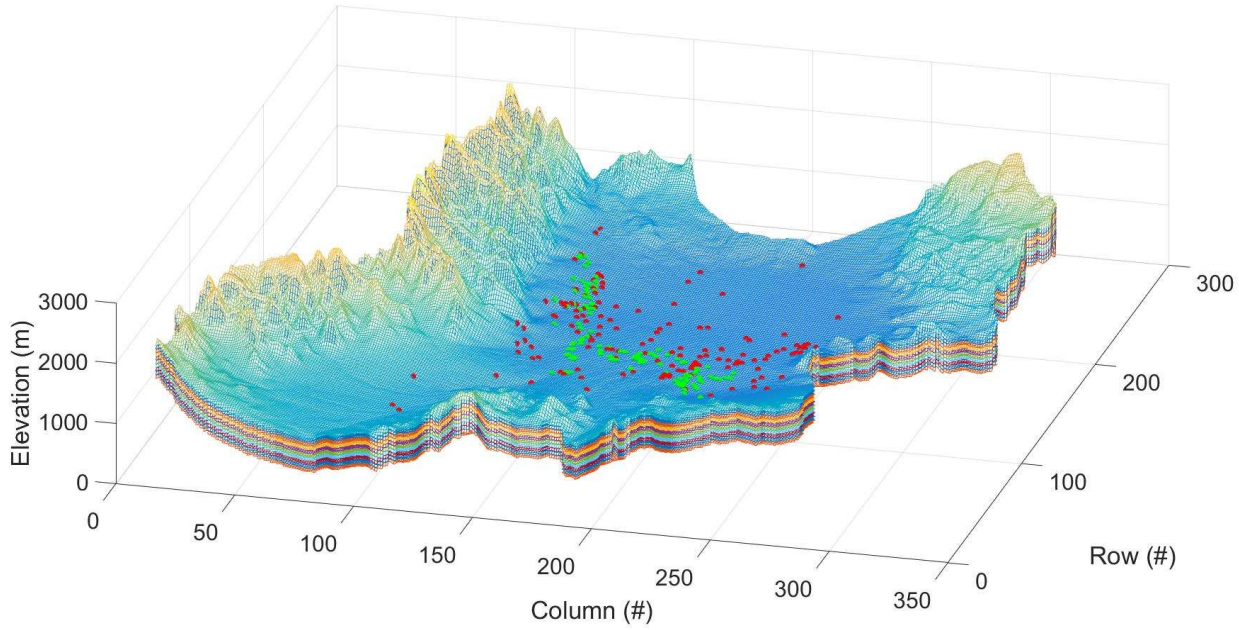

Figure 2.6 – The IWV model was divided into 10 layers with a terrain following grid approach. The mesh was subsequently refined to exclusively include the topographic depression (i.e. aquifer extent). The remaining cells were set to no-flow cells, however the MFR these areas would contribute was calculated and applied as a boundary condition for saturated zone model. The green dots represent the pumping wells within the basin, and the red dots represent the locations for which groundwater elevation data were available between 1985 – present. These data were subsequently used for calibration.

2.4.2 Boundary Conditions and Hydrologic Flux Development

Boundary conditions for the groundwater model were defined by the bedrock-basin-fill interface at the outer extent of the IWV topographic depression within the delineated watershed. The resulting space between the watershed boundaries and the groundwater model boundaries were treated as no-flow cells, with recharge occurring on the model boundaries. Recharge values applied to the model boundaries were derived from the difference between monthly 30-year average precipitation (i.e. PRISM product) and the 15-year average of monthly SSEBop ET product (Figure 2.7). Recharge was only applied at model boundaries because all precipitation falling within the IWV is assumed to evaporate prior to infiltration, as supported by SSEBop and PRISM data (Figure 2.7). Consequently, the boundary conditions were modeled to represent the MFR occurring from precipitation falling in the mountains and infiltrating into the IWV aquifer.

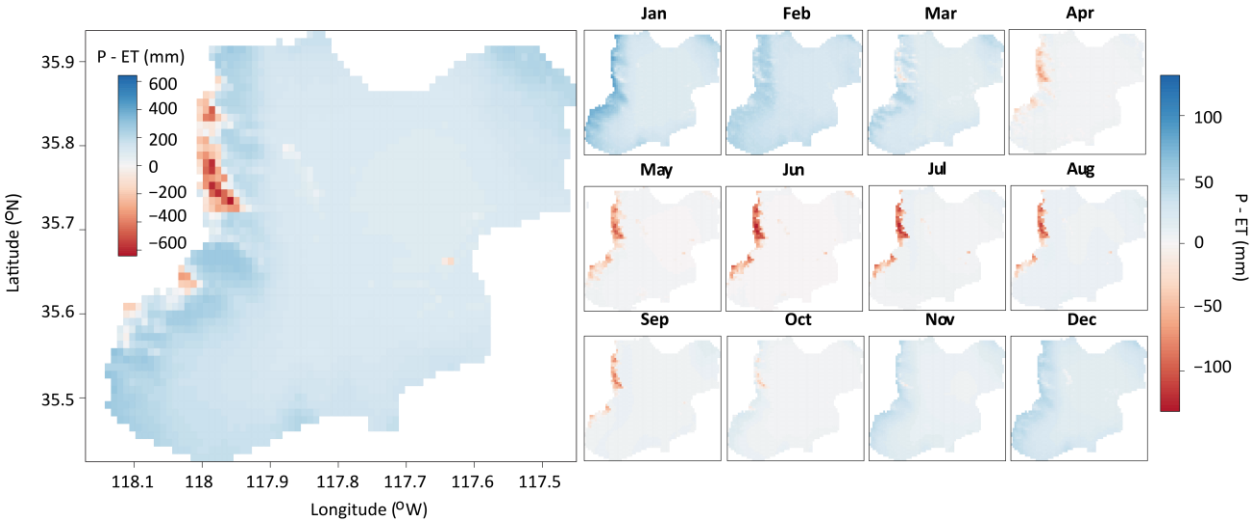

Figure 2.7 - The difference between the PRISM dataset and the SSEBop dataset. The larger figure on the left is the annual difference; monthly differences are on the tiles to the right. The seasonal wet and dry periods coincide with the precipitation data presented in Figure 4. The higher negative monthly rates indicate loss of snowpack in the Sierra Nevada during the summer months.

The gridded ET product was subtracted from PRISM precipitation product in the cells outside of the model boundary. The resulting values were averaged by mountain range (e.g. Sierra Nevada, Coso, Argus, El Paso), and used to populate initial MFR values for the model. This was accomplished by summing the total difference between precipitation and ET for all

cells in each of the bordering mountain ranges outside the active model domain. This sum was then distributed evenly along the models boundary cells for each mountain range.

Current water use was obtained from the Kern County Water Agency with the spatial location of groundwater wells, and their monthly pumping rates (Michelle Anderson, personal communication, 5/9/15). Groundwater pumping rates combined with ET constrained to the spatial extent of the China Lake playa encompass the two hydrologic outputs from the model. Consequently, the conceptual mass balance for the model consists of inputs from MFR from each of the surrounding mountain ranges, and water removed via pumping and ET at the China Lake playa.

2.4.3 Model Calibration

Groundwater elevation values exist from 1920 to present at over 200 different wells across the IWV (Figure 9); however, a majority of the data exists only from 1985 to present. Consequently, the model calibration period began in 1985, ignoring previous data.

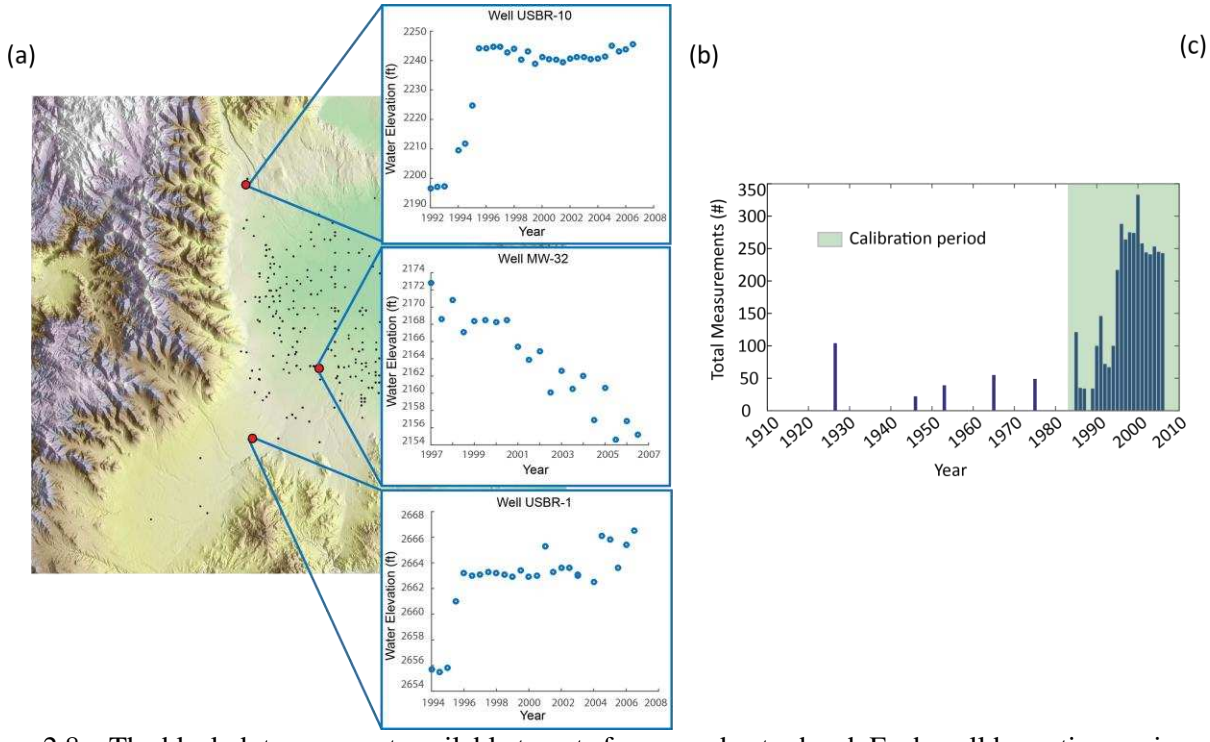

Figure 2.8 – The black dots represent available targets for groundwater head. Each well has a time series of data used for calibration (center). A majority of the data existed between 1985 to 2005, consequently this time period was used for model calibration.

Using the calculated MFR values and simulated lithology distributions, the model was calibrated from 1985 to 2006 using measured groundwater elevation data for each respective year (3327 measurements in total). Specifically, PEST was used optimize four hydraulic conductivity values (i.e one for each lithology), five recharge zones, as well as the evapotranspiration rate and the maximum depth the water table was allowed to reach before it was assumed that ET was negligible (i.e extinction depth). Input PEST files can be found in Appendix A, other PEST files have been uploaded separately. Model recharge zones are model boundaries with uniform recharge rates within the zone, each zone was calibrated, and a single value was assigned to each zone. The goodness of model fit was assessed using metrics commonly employed for groundwater model calibration including: (1) the correlation coefficient of observed versus simulated groundwater heads; (2) the mean residuals between the observed and modeled heads in the model simulation; (3) the root-mean-square error (RMSE) between observed and simulated heads; and (4) the scaled RMSE adjusted for the difference between the maximum and minimum observation head.

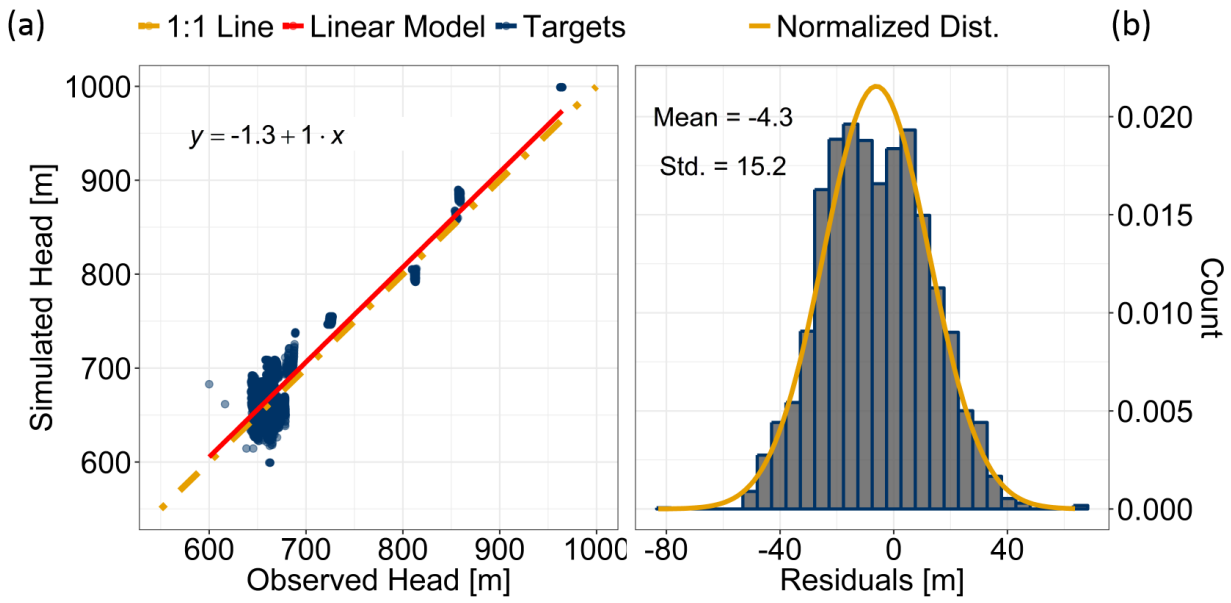

Figure 2.9 – Observed versus simulated head measurements were plotted against a 1:1 line representing a perfect model calibration (left). Additionally, a linear regression model was fit the data and compared to the ideal 1:1 line. At right, the model residuals are plotted as a histogram against a normal distribution with the same mean and variance as the model residuals; the mean model residual is -4.3 meters.

The final calibrated model displayed a linear regression model fit visually similar to the 1:1 line (Figure 10a), a nearly-normal distribution of residuals with a mean of -4.3m and a standard deviation of 15.2m (Figure 10b), and a scaled RMSE of 0.05 m (Figure 11). In total, five separate PEST runs were conducted, each run with a decreasing allowance for observed error. PEST runs were ceased once subsequent error reductions became less than 1%. Inversion parameters were set to ensure that variables stayed within reasonable bounds and ratios. Specifically, for each lithology specific yield and hydraulic conductivity values were constrained to the maximum and minimum values reported common for the lithology [*Fetter*, 2001], and both ET and recharge values were allowed to vary +/- 20%, which was in-line with regional averages.

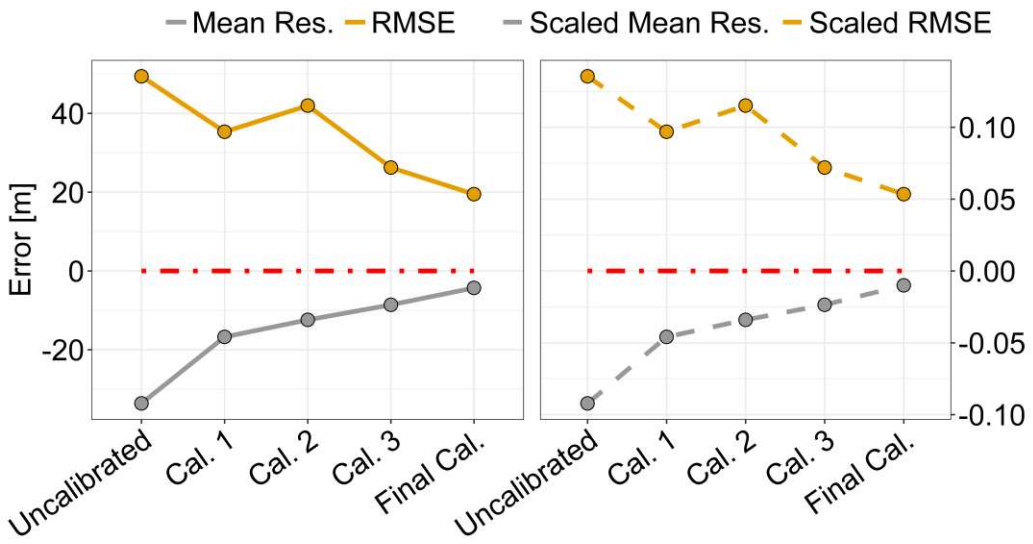

Figure 2.10 – Scaled (right) and unscaled (left) model error results. Scaled error results are the original error statistic divided by the difference between the lowest and highest target head within the basin.

After the final iteration was complete, model residuals were compared at each grid cell's X and Y coordinates as well as through time. Each comparison produced Pearson correlation coefficients below 0.1, suggesting that there was not a strong correlation between model residuals and target locations, or model timesteps. Therefore, it was concluded that there were not strong spatial or temporal biases within the model.

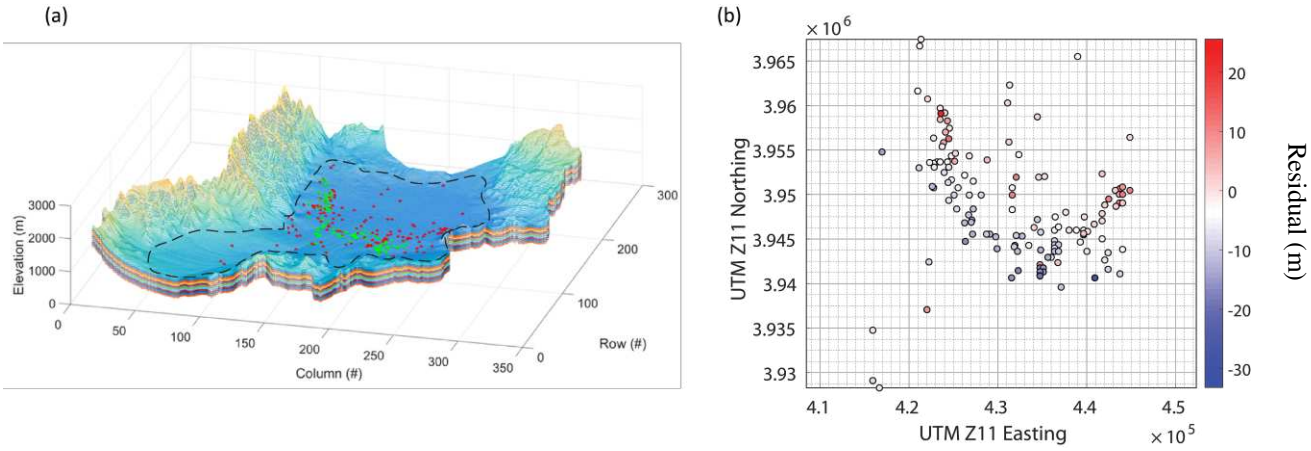

Figure 2.11 – (a) The model boundaries (dotted line), with target wells in green; (b) an area map of residuals in meters with red being high residual values and blue being low residual values.

Additionally, the cumulative sum of residuals was plotted to ensure that several targets were not responsible for a majority of model error, and residual distribution was plotted and compared against a standard normal distribution in order to further determine potential bias in model residuals (Figure 2.10b).

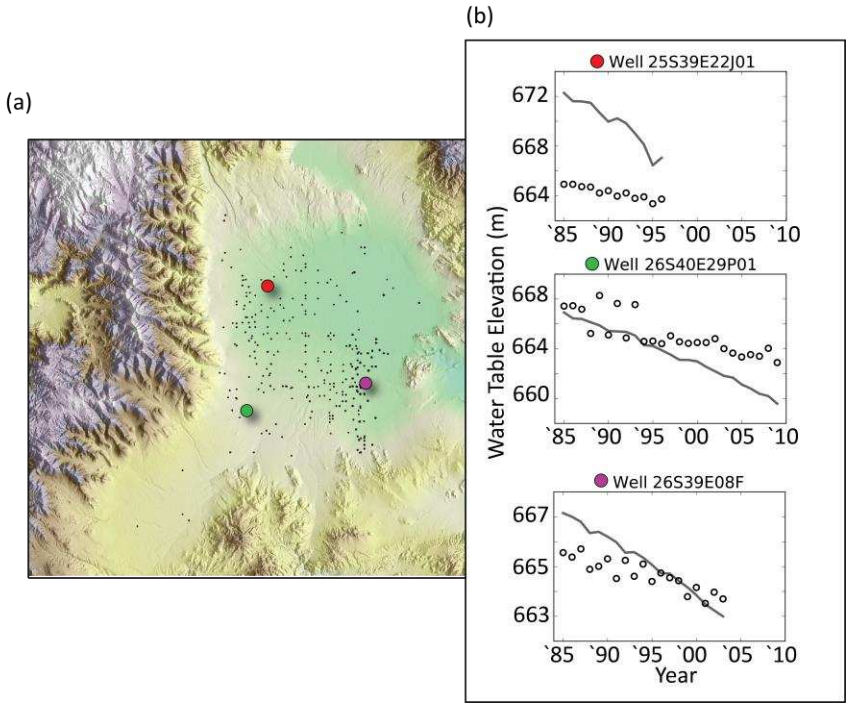

Figure 2.12 – Part (a) shows the location of the calibration time series plotted. Part (b) shows the time-series of observed heads (circles) and simulated heads (line) for three wells in different parts of the IWV. Generally they replicate the trend of falling groundwater elevation, however simulated condition fall at a faster rate than those observed.

2.4.4 Future Scenario Development

Once the model was calibrated, the land-surface area, energy use, and water use of potential renewable energy technologies were accounted for. Specifically, the renewable fuel types considered included PV, CSP, wind, and biofuel. It should be noted that these implementations were not considered for the entire life cycle of the renewable project. For example, the water and energy needed to create a wind turbine was not accounted for; instead, water, energy, and land use associated with operation was considered exclusively.

Table 2.1 – Total energy use per year in Megawatt-hours (MWh) for Kern County. Values specific to the IWV were not available; instead, values here represent average values for use per person within Kern County scaled to the population of the IWV.

Year	Non-Residential (MWh)	Residential (MWh)	Total (MWh)	Kern County Pop.	IWV Pop.	IWV Use (MWh)
2015	12775	2296	15071	882176	28715	640
2014	10890	2299	13189	874190	30170	647
2013	12748	2273	15021	865787	31625	644
2012	14413	2276	16690	856576	33080	548
2011	13803	2143	15946	849949	34535	455
2010	12852	2096	14949	839631	35990	490

To determine the energy each fuel type needs to generate to provide electricity for the IWV, yearly energy use for Kern County was obtained from the California Energy Commission. Data were obtained for years 2010 through 2015 for residential, nonresidential, and total energy usage. The total energy usage was subsequently divided by the total population of Kern County for each respective year (also obtained from www.energy.ca/gov). This provided an estimate of yearly energy usage per person for Kern County for each year between 2010 and 2015.

Based on this usage, the amount of water needed to provide the IWV with 100% of their total generation was calculated for each fuel type. 100% of total generation was chosen to provide a ceiling for maximum impact, producing highly conservative model results. Values from previous review studies conducted by the National Renewable Energy Laboratory [*Ong et al.*, 2013] provided estimates of water used in gallons per MWh per year for each fuel type. With

yearly estimates of IWV energy use converted to MWh, we calculated the total gallons of water needed for the years of 2010 – 2015 for each renewable fuel type listed above.

Unlike PV and wind solutions, CSP and biomass implementations rely on different cooling technologies for electrical generation, resulting in a large spectrum of water use (Table 2; Figure 14). This is because the two technologies rely on sun (CSP) or biomass (biofuels) to heat a fluid, and power steam-driven turbines. Consequently, minimum, median and maximum values for water use were simulated for each major cooling and circulation technology within the CSP and biomass fuel types. Based on the minimum, median, and maximum energy use for each renewable scenario, the minimum, average and maximum land use was calculated. Land-cover and land-use types were obtained from the National Landcover Database, and the California Department of Water Resources (http://www.water.ca.gov/). Based on the land use needed for each renewable implementation scenario, a region within public land available in the IWV was selected.

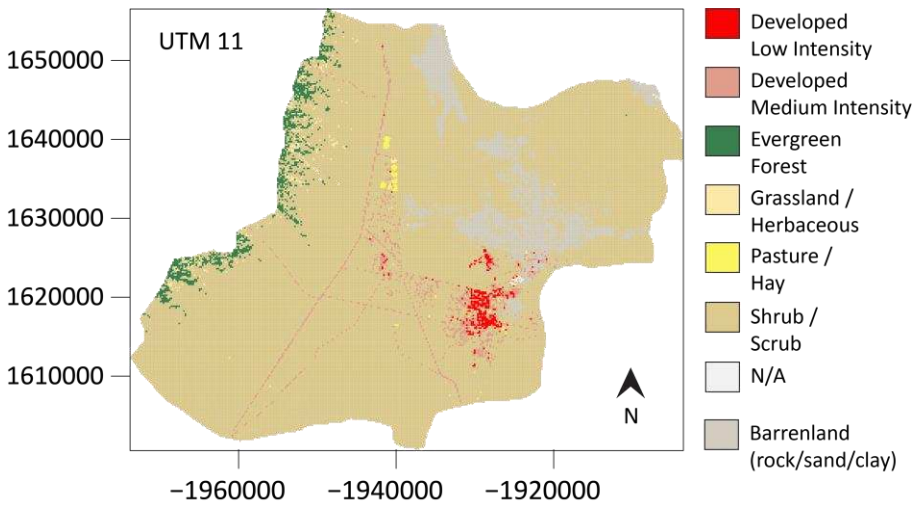

Figure 2.13 - 2011 National Landcover Database land-cover and land-use data for the IWV [Homer et al., 2015]. These data were used to identify suitable locations for potential renewable implementations based on each scenario's land-footprint.

Water was pumped from the implementation site at a rate commensurate with the water use calculated for each implementation scenario above. Drawdown from the model was observed at the pumping well, as well as in adjacent observation wells at distances of 200 and 400 m to the north, east, south, and west. These drawdown curves were used to determine the extra energy

needed to pump water to the ground surface, since no perennial surface water is available within the IWV. The energy required for groundwater pumping was dependent on the amount of water pumped, and the distance that water needed to be lifted. It should be noted that friction within the pumping well was neglected, and the pump was considered to be operating at 100% efficiency. Therefore, the energy-use values reported are considered conservative. Groundwater availability is expected to decrease in the southwestern U.S. under a changing climate [*Taylor et al.*, 2013; *Thomas and Famiglietti*, 2014; *Meixner et al.*, 2015]. Additionally, the IWV is using more groundwater than is currently replenishing the aquifer, leading to yearly groundwater decline (IWVWD, 2016, http://www.iwvwd.com/public-documents/public-reports/). To assess the hydrologic impact and the extra energy that would be needed to power the renewable scenarios derived above, the same scenarios were run with a 5%, 10%, and 20% percent decrease in recharge, assuming that the groundwater use within the basin remains consistent. We note that this assumption may not be valid under the observed population growth in the IWV, or with water conservation efforts, but allows for different renewable scenarios to be modeled under potential future conditions.

2.5 Results

Water use for each of the renewable energy implementations varies across a large spectrum (Figure 13). The CSP solution has the largest hydrologic impact, followed by biomass, PV, and wind-powered solutions. The high water use associated with biopower and CSP solutions are a direct result of them leveraging thermoelectric power-generation techniques, with the major difference being the fuel source used to heat the circulating fluid. On the lower side of water consumption, PV implementations have a higher water use than wind due to the need for dust suppression, and maintaining clean panels for maximum efficiency. Solar panels lose efficiency when particulate reduces the surface area that is absorbing solar radiation.

Land use did not directly coincide with water use. Specifically, wind power solutions required much larger land footprints on average with PV, CSP, and biofuel solutions having similar land use requirements [*Ong et al.*, 2013]. Water was pumped from the identified implementation location at rates commensurate with the identified water use above. Drawdowns are substantially larger for CSP and biofuel implementations because they require substantially larger pumping rates than other energy types. Specifically, cones of depression between 8 and 60 m were observed in the pumping wells for all runs.

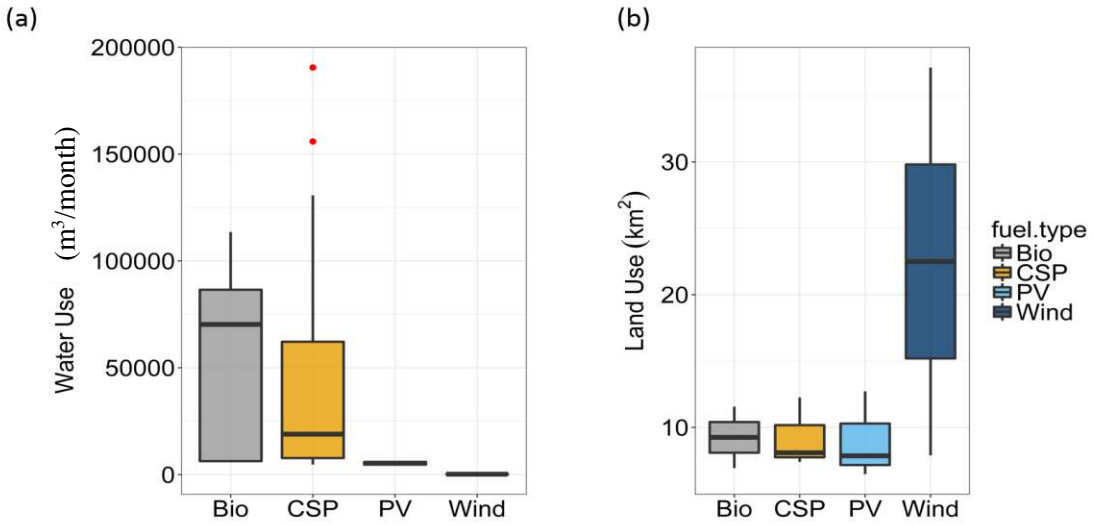

Figure 2.14 – Water use for each energy-generating technology to meet the IWV's monthly energy demand, derived from water-use rates calculated from Macknick et al. [2012a]. Biofuel and concentrating solar plants (CSP) have the highest water use rates amongst the four generation technologies considered.

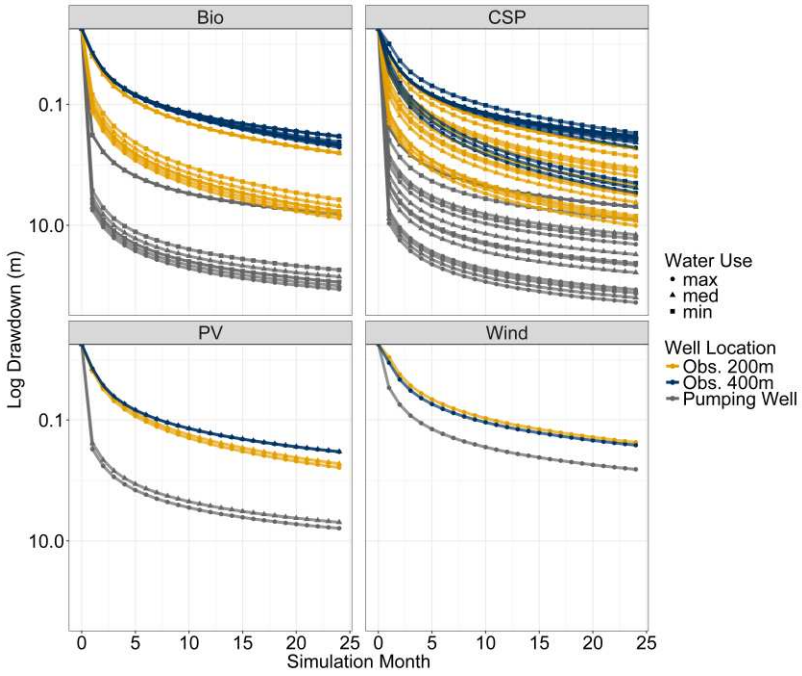

Figure 2.15 – Drawdown curves for each realization (baseline, 5%, 10%, and 20% decrease in MFR) are plotted above. Yearly water use rates were divided up evenly between months of the year and applied as steady-state pumping over a two-year model simulation. The resulting cones of depression are presented for minimum, median, and maximum water use rates for each technology. It is immediately apparent that PV and wind technologies have the smallest cone of depression associated with water use, followed by biofuel and CSP technologies.

The largest water withdrawals resulted in larger cones of depression, and consequently larger amounts of energy needed to lift this water out of the ground. When MFR was decreased by 5, 10, and 20% from the adjacent mountain ranges, final solution heads decreased by 3, 6, and 10 m at the pumping well. The decrease in simulated groundwater resulted in increased energy use needed to retrieve the needed water by 0.5 to 3% over a two-year period depending on the fuel type and cooling technology (Figure 16); consequently, the net productivity (i.e. total electricity generated – total electricity used to pump water from wells) of each of the respective simulations decreased. This means that under a changing climate, assuming decreased MFR as has been predicted by Meixner et al. (2016), we will see a depressed water table in SWBR such that renewable implementations will require more water and land-surface area to maintain the same efficiencies expected during implementation (Figure 16).

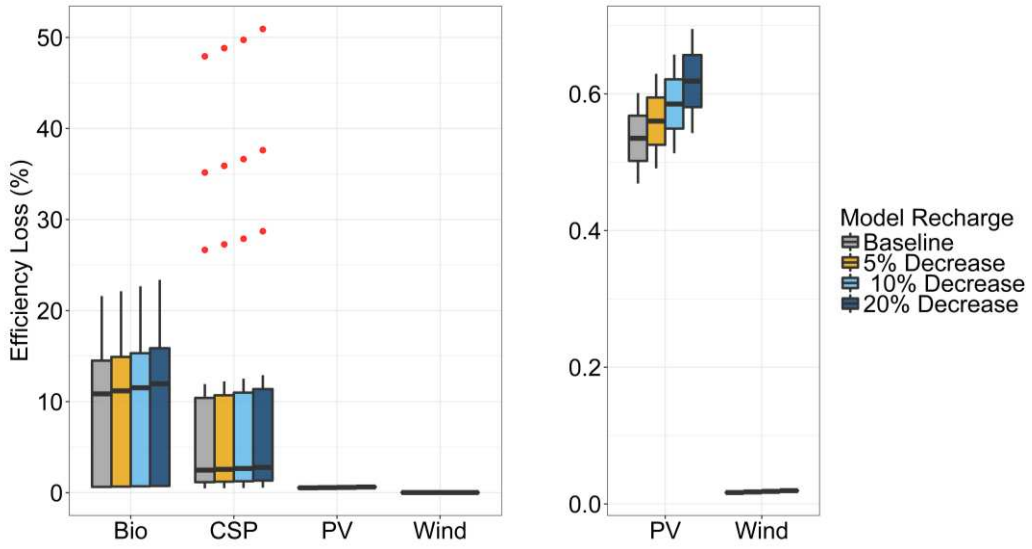

Figure 2.16 – The energy required to pump groundwater to supply each scenario's water needs was subtracted from the total energy generated by each technology. This was done for the baseline scenario as well as future scenarios with decreased MFR rates where model recharge was decreased by 5, 10 and 20%. Cones of depression induced by biofuel and CSP technologies can result in significant efficiency losses.

While it is important to know the total baseline use for each implementation scenario, metrics that are more useful for expressing hydrologic impact are (1) the water use for each scenario expressed as a fraction of total water used in the IWV; and (2) the water use for each scenario expressed as a fraction of total aquifer recharge. Biomass resulted in almost 4% of water

used to total water? in the basin and CSP accounted for 2% (Figure 17). Both the PV and wind solutions accounted for a negligible amount of pumping within the IWV.

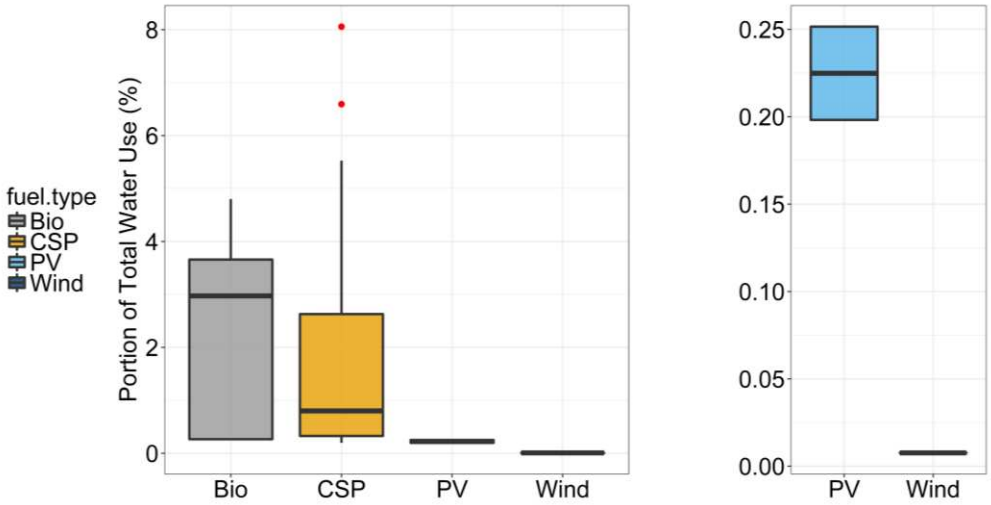

Figure 2.17 – Total reported water use (IWVWD, 2016, http://www.iwvwd.com/public-documents/public-reports/) within the IWV was used to scale the percentage of total water use within the basin that each scenario would account for. All median values fell below 4%, with CSP, wind and PV falling below 1%.

Additionally, water use was calculated as a fraction of total recharge. For this, all the recharge values previously derived for the IWV [*Kunkel and Chase*, 1969; *Bloyd and Robson*, 1971; *Moyle and Dutcher*, 1973; *Berenbrock and Martin*, 1991] including the ones from this study, were used for comparison. Most of the values are in the same ranges (Figure 18); however, several values are tiny as a result of these studies suggesting that the IWV is an open basin with high recharge rates.

Some types of biofuel and CSP implementations have the potential to would consume a large volume of water for operational needs, accounting for a significant portion of total precipitation within the basin. Expressing the volume consumed by each scenario as a fraction of the basin's total precipitation is a more representative metric than water volume use alone because each aquifer can support different volumes of water use based on how much recharge is received. Some renewable implementations were found to have a smaller, or no adverse impact in the IWV than others based on: (1) water impact; (2) energy impact; and (3) land-area impact (Figure 13). It was concluded that: (1) wind has the largest land impact but the lowest water impact; (2) CSP and biofuel implementations have similar water use, land use, and net efficiency values, with differences depending on the cooling type; (3) PV solutions have a similar land

footprint to CSP and biofuel technologies, but uses substantially less water. Consequently, PV would be the best balance between water and land-use for the IWV, and for groundwater dependent basin-and-range settings. In areas with limited water resources but abundant available land for implementation, wind would be a good solution.

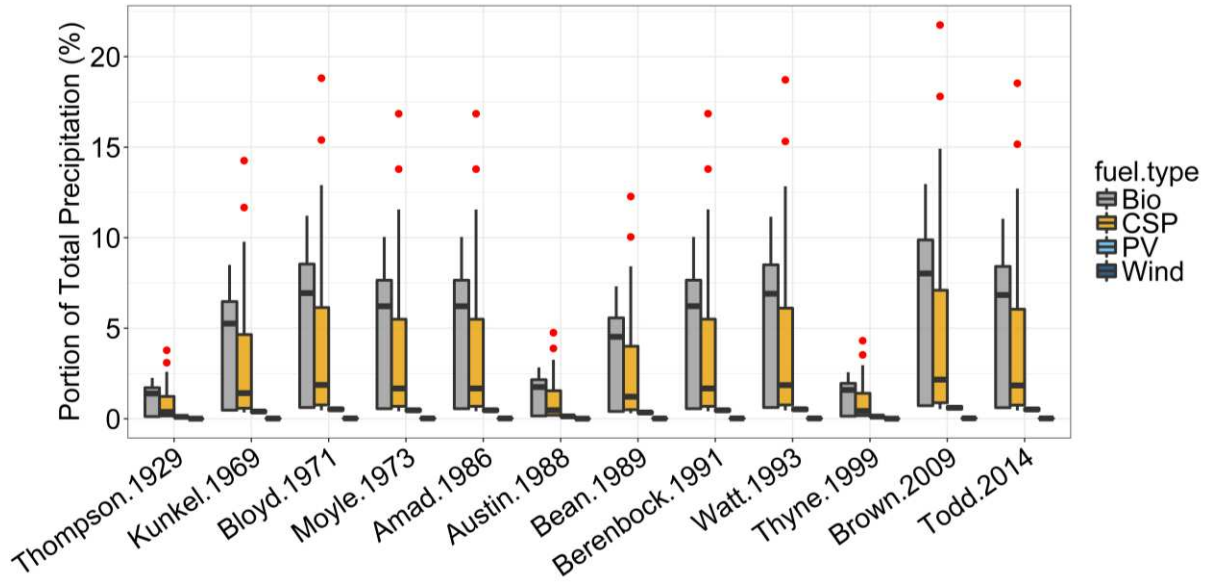

Figure 2.18 – Water use for each generation technology was plotted as a function of estimated basin recharge. Existing literature values were used, as well as values from this study. Two distinct patterns can be seen above; specifically, studies assuming an open basin estimated substantially larger recharge values, and consequently water used by each implementation scenario is much lower than this study, and the majority of existing research.

However, the one advantage of thermoelectric generation is that heat is used to create electricity, and consequently heat can be stored, providing a lag time between available energy (as heat) and energy use to generate electricity. This is not available in PV or wind implementations, which directly convert incoming solar radiation to electricity, electricity that is lost immediately if not used or stored. This complicates the integration of PV and WT into electrical grids where demand exists during non-sunny or non-windy periods of time.

As observed above, the need to pump groundwater in regions with no perennial surface water can lead to large cones of depression that greatly decrease the net efficiency of renewable implementations. Over the two-year simulation, efficiency loss increased by 2-5% for a 5%, 10%, and 20% decrease in MFR. Under a changing climate, continually falling groundwater tables have the potential to lead to significant losses over longer periods of time than the current model simulation. This has the potential to increase the land footprint for renewables needing to

generate a specific quantity of electrical energy. Additionally, continually falling groundwater tables as a function of anthropogenic withdrawals will have a similar effect. How these two variables feedback to shape future renewable energy implementations, and the feasibility of utility-scale implementation in groundwater-dependent desert ecosystems based on those feedbacks, remains unclear.

2.6 Conclusions

Renewable energy solutions will play an increasingly important role in balancing future energy and water demands. However not all renewable energy solutions have similar impacts; the balance between land-use, water-use, and energy production is different amongst different renewable energy fuel types and technologies. Here, suites of implementation scenarios were created to capture variability water use, and evaluate potential hydrologic and land-surface impacts of each implementation type. Of all the proposed scenarios, wind and PV had the lowest water impact, while CSP and biofuels had the largest. Additionally, the projected water use for CSP and biopower scenarios were highly variable depending on the cooling and circulation technology used in the thermoelectric generation process, a process not needed by wind or PV implementations. In terms of land-surface impact, wind required the largest implementation area, with PV, CSP and biopower all having similar land-surface footprints.

A numerical model of the IWV aquifer was calibrated to existing groundwater elevation data and used to simulate the water withdrawals expected for each scenario. This provided the ability to quantify potential human-induced groundwater change for energy development under current and simulated future conditions. Future conditions were created to reproduce aquifer conditions where MFR values decreased, a predicted result of climate change in SWBR settings. Specifically, MFR values were decreased by, 5, 10, and 20% resulting in a 3, 6, and 10 m local decrease in the groundwater table near the implementation site. Cones of depression from pumping at the implementation site ranged between 8 and 60 m, with wind and PV having the smallest impact. Water use was expressed in terms of total estimated recharge, and the extra energy required to pump groundwater at the implementation site was calculated. It was concluded that biofuel and CSP implementations have the potential to consume a significant portion of the water recharging the IWV aquifer annually, and that these impacts are a function of cooling and circulation technologies used than fuel types implemented. In addition to the total amount of water used, the decrease in simulated groundwater elevation resulted in a larger

energy demand to extract groundwater at the implementation site. The energy use needed to extract groundwater for implementation scenarios increased by 0.5 to 3% during the simulation period. This increase was a function of the fuel type and cooling technology driving the amount of water required for each scenario.

For the IWV, and other SWBR settings where even small quantities of water use can be a limiting factor to implementation, PV solutions would provide the most beneficial balance between water and land-use. In SWBR settings where water resources are so limited that PV solutions are not feasible, wind scenarios would be a good solution. If a changing climate in SWBR causes continually falling groundwater tables, there is potential for significant efficiency losses over longer periods of time. These losses would increase the land footprint required to achieve the same net electrical generation as the same implementation would under current hydrologic conditions. The future state of hydrologic conditions in SWBR setting are uncertain; however, by quantifying the water needs of renewable scenarios and modeling their impact using a hydrologic model, water managers can assess potential future impacts and the future efficiency of potential implementations under a variety of predicted future conditions.

REFERENCES

AghaKouchak, A., L. Cheng, O. Mazdiyasni, and A. Farahmand (2014), Global warming and changes in risk of concurrent climate extremes: Insights from the 2014 California drought, *Geophys. Res. Lett.*, *41*(24), 2014GL062308, doi:10.1002/2014GL062308.

Bales, R. C., N. P. Molotch, T. H. Painter, M. D. Dettinger, R. Rice, and J. Dozier (2006), Mountain hydrology of the western United States, *Water Resour. Res.*, *42*(8), doi:10.1029/2005WR004387.

Barnett, T. et al. (2008), Human-induced changes in the hydrology of the western United States., *Science (80-.).*, *319*(5866), 1080–1083, doi:10.1126/science.1152538.

Bazilian, M. et al. (2011), Considering the energy, water and food nexus: Towards an integrated modelling approach, *Energy Policy*, *39*(12), 7896–7906, doi:10.1016/j.enpol.2011.09.039.

Berenbrock, C., and P. Martin (1991), THE GROUND-WATER FLOW SYSTEM IN INDIAN WELLS VALLEY , KERN , INYO , AND SAN BERNARDINO COUNTIES , CALIFORNIA, *USGS*.

BLM (2012), Approved Resource Management Plan Amendments / Record of Decision (ROD) for Solar Energy Development in Six Southwestern States, , (October).

Bloyd, R. M., and S. G. Robson (1971), MATHEMATICAL GROUND-WATER MODEL OF INDIAN WELLS VALLEY, CALIFORNIA, *USGS Rep.*

Brown, R. D., and D. A. Robinson (2011), Northern Hemisphere spring snow cover variability and change over 1922-2010 including an assessment of uncertainty, *Cryosphere*, *5*(1), 219–229, doi:10.5194/tc-5-219-2011.

Brutsaert, W. (2006), Indications of increasing land surface evaporation during the second half of the 20th century, *Geophys. Res. Lett.*, *33*(20), 1–4, doi:10.1029/2006GL027532.

Cayan, D. R., E. P. Maurer, M. D. Dettinger, M. Tyree, and K. Hayhoe (2007), Climate change scenarios for the California region, *Clim. Change*, *87*(1 SUPPL), doi:10.1007/s10584-007-9377-6.

Christensen, N. S., A. W. Wood, N. Voisin, D. P. Lettenmaier, and R. N. Palmer (2004), The effects of climate change on the hydrology and water resources of the Colorado River basin, *Clim. Change*, *62*(1–3), 337–363, doi:10.1023/B:CLIM.0000013684.13621.1f.

Cook, B. I., J. E. Smerdon, R. Seager, and S. Coats (2014a), Global warming and 21st century drying, *Clim. Dyn.*, 1–21, doi:10.1007/s00382-014-2075-y.

Cook, B. I., R. Seager, and J. E. Smerdon (2014b), The worst North American drought year of the last millennium : 1934, *Geophys. Res. Lett.*, *41*, 1–8, doi:10.1002/2014GL061661.Received.

Cook, E. R., C. A. Woodhouse, C. M. Eakin, D. M. Meko, and D. W. Stahle (2004), Long-Term Aridity Changes in the Western United States, *Science (80-.).*, *306*(5698), 1015–1018, doi:10.1126/science.1102586.

Dai, A. G. (2013), Increasing drought under global warming in observations and models, *Nat. Clim. Chang.*, *3*(1), 52–58, doi:10.1038/nclimate1633.

Daly, C., C. Neilson, and D. Philips (1994), A Statistical-Topographic Model for Mapping Climatological Precipitation over Mountainous Terrain, *J. Appl. Meteorol.*

Daly, C., W. P. Gibson, G. H. Taylor, G. L. Johnson, and P. Pasteris (2002), A knowledge-based approach to the statistical mapping of climate, *Clim. Res.*, *22*(2), 99–113, doi:10.3354/cr022099.

Daly, C., M. Halbleib, J. I. Smith, W. P. Gibson, M. K. Doggett, G. H. Taylor, and P. P. Pasteris (2008), Physiographically sensitive mapping of climatological temperature and precipitation across the conterminous United States, *Int. J. Climatol.*, *2064*(March), 2031–2064, doi:10.1002/joc.

Famiglietti, J. S. (2014), The global groundwater crisis, *Nat. Clim. Chang.*, *4*(11), 945–948, doi:10.1038/nclimate2425.

Famiglietti, J. S., M. Lo, S. L. Ho, J. Bethune, K. J. Anderson, T. H. Syed, S. C. Swenson, C. R. De Linage, and M. Rodell (2011), Satellites measure recent rates of groundwater depletion in California's Central Valley, *Geophys. Res. Lett.*, *38*, 2–5, doi:10.1029/2010GL046442.

Fetter, C. W. (2001), Applied Hydrogeology, , 598.

Foster, L., L. Bearup, N. Molotch, P. Brooks, and R. Maxwell (2016), Energy budget increases reduce mean streamflow more than snow–rain transitions: using integrated modeling to isolate climate change impacts on Rocky Mountain hydrology, *Environ. Res. Lett.*, *11*(4), 44015, doi:10.1088/1748-9326/11/4/044015.

Godsey, S. E., J. W. Kirchner, and C. L. Tague (2014), Effects of changes in winter snowpacks on summer low flows: Case studies in the Sierra Nevada, California, USA, *Hydrol. Process.*, *28*(19), 5048–5064, doi:10.1002/hyp.9943.

Griffin, D., and K. J. Anchukaitis (2014), How unusual is the 2012-2014 California drought?, *Geophys. Res. Lett.*, *41*(24), 9017–9023, doi:10.1002/2014GL062433.

Indian Wells Valley Water District (IWVWD), www.iwvwd.com.

Hao, Z., A. AghaKouchak, N. Nakhjiri, and A. Farahmand (2014), Global integrated drought monitoring and prediction system, *Sci. Data*, *1*, 1–10, doi:10.1038/sdata.2014.1.

Hartmann, D. L. (2015), Pacific sea surface temperature and the winter of 2014, *30, 1092*, 1–9, doi:10.1002/2015GL063083.Received.

Healy, R. W., W. M. Alley, M. A. Engle, P. B. McMahon, and J. D. Bales (2015), *The Water-Energy Nexus — An Earth Science Perspective Circular 1407.*

Homer, C. G., J. A. Dewitz, L. Yang, S. Jin, P. Danielson, G. Xian, J. Coulston, N. D. Herold, J. D. Wickham, and K. Megown (2015), Completion of the 2011 National Land Cover Database for the conterminous United States-Representing a decade of land cover change information, *Photogramm. Eng. Remote Sensing*, *81*(5), 345–354, doi:10.14358/PERS.81.5.345.

Kunkel, F., and G. H. Chase (1969), GEOLOGY AND GROUND WATER IN INDIAN WELLS VALLEY, CALIFORNIA, *USGS.*

Leake, S. A., and A. D. Konieczki (2000), Ground-Water Resources For the Future: Desert Basins of the Southwest, *U.S. Geol. Surv.*, (August).

Leonard, M., S. Westra, A. Phatak, M. Lambert, B. van den Hurk, K. Mcinnes, J. Risbey, S. Schuster, D. Jakob, and M. Stafford-Smith (2014), A compound event framework for understanding extreme impacts, *Wiley Interdiscip. Rev. Clim. Chang.*, *5*(1), 113–128, doi:10.1002/wcc.252.

Lewis, N. S. (2007), Toward Cost Effective Solar Energy Use, *Science (80-.).*, *798*(2007), 798–802, doi:10.1126/science.1137014.

Luce, C. H., J. T. Abatzoglou, and Z. a Holden (2013), The missing mountain water: slower westerlies decrease orographic enhancement in the Pacific Northwest USA., *Science (80-.).*, *342*(6164), 1360–4, doi:10.1126/science.1242335.

Di Luzio, M., G. L. Johnson, C. Daly, J. K. Eischeid, and J. G. Arnold (2008), Constructing retrospective gridded daily precipitation and temperature datasets for the conterminous United States, *J. Appl. Meteorol. Climatol.*, *47*(2), 475–497, doi:10.1175/2007JAMC1356.1.

MacDonald, G. M. (2010), Water, climate change, and sustainability in the southwest, *Proc. Natl. Acad. Sci.*, *107*(50), 21256–21262, doi:10.1073/pnas.0909651107.

Macknick, J., R. Newmark, G. Heath, and K. C. Hallett (2012a), Operational water consumption and withdrawal factors for electricity generating technologies: a review of existing literature, *Environ. Res. Lett.*, *7*(4), 45802, doi:10.1088/1748-9326/7/4/045802.

Macknick, J., S. Sattler, K. Averyt, S. Clemmer, and J. Rogers (2012b), The water implications of generating electricity: water use across the United States based on different electricity pathways through 2050, *Enviromental Res. Lett.*, doi:10.1088/1748-9326/7/4/045803.

Markovich, K. H., R. M. Maxwell, and G. E. Fogg (2016), Hydrogeological response to climate change in alpine hillslopes, *Hydrol. Process.*, *30*(18), 3126–3138, doi:10.1002/hyp.10851.

Maupin, M. A., J. F. Kenny, S. S. Hutson, J. K. Lovelace, N. L. Barber, and K. S. Linsey (2014), *Estimated use of water in the United States in 2010.*

Meixner, T. et al. (2015), Implications of Projected Climate Change for Groundwater Recharge in the Western United, *J. Hydrol.*, *534*, 124–138, doi:10.1016/j.jhydrol.2015.12.027.

Monastero, F. (2002), Neogene Evolution of the Indian Wells Valley, east-central California, *GSA Mem.*

Moyle, W. R., and L. C. Dutcher (1973), Geologic and Hydrologic Features of Indian Wells Valley , Geologic and Hydrologic Features of Indian Wells Valley , California, *USGS*.

Mu, Q., M. Zhao, and S. W. Running (2013), MODIS Global Terrestrial Evapotranspiration (ET) Product (MOD16A2/A3) - ATBD Collection 5, , 66.

Ong, S., C. Campbell, P. Denholm, R. Margolis, and G. Heath (2013), Land-Use Requirements for Solar Power Plants in the United States, *Nrel/Tp-6a20-56290*, (June), 47.

Remy, N., A. Boucher, and J. Wu (2009), *Applied Geostatistics with SGeMS: A User's Guide*.

Robeson, S. M. (2015), Revisiting the recent California drought as an extreme value, , 1–9, doi:10.1002/2015GL064593.Received.

Seager, R., and M. Hoerling (2014), Atmosphere and ocean origins of North American droughts, *J. Clim.*, *27*(12), 4581–4606, doi:10.1175/JCLI-D-13-00329.1.

Seager, R. et al. (2007), Model projections of an imminent transition to a more arid climate in southwestern North America., *Science*, *316*(5828), 1181–4, doi:10.1126/science.1139601.

Seager, R., M. Hoerling, S. Schubert, H. Wang, B. Lyon, A. Kumar, and J. Nakamura (2015), Causes and Predictability of the 2011-14 California Drought, *NOAA Drought Task Force Assess. Rep.*, doi:10.7289/V7258K7771F.

Senay, G. B., S. Bohms, R. K. Singh, P. H. Gowda, N. M. Velpuri, H. Alemu, and J. P. Verdin (2013), Operational Evapotranspiration Mapping Using Remote Sensing and Weather Datasets: A New Parameterization for the SSEB Approach, *J. Am. Water Resour. Assoc.*, *49*(3), 577–591, doi:10.1111/jawr.12057.

Sherwood, S., and Q. Fu (2014), A Drier Future?, *Science (80-.).*, *343*(6172), 737–739, doi:10.1126/science.1247620.

Shukla, S., M. Safeeq, A. Aghakouchak, K. Guan, and C. Funk (2015), Temperature impacts on the water year 2014 drought in California, , 1–10, doi:10.1002/2015GL063666.Received.

Singh, R. K., G. B. Senay, N. M. Velpuri, S. Bohms, R. L. Scott, and J. P. Verdin (2013), Actual evapotranspiration (water use) assessment of the colorado river basin at the landsat resolution using the operational simplified surface energy balance model, *Remote Sens.*, *6*(1), 233–256, doi:10.3390/rs6010233.

Stewart, I. T., D. R. Cayan, and M. D. Dettinger (2005), Changes toward earlier streamflow timing across western North America, *J. Clim.*, *18*(8), 1136–1155, doi:10.1175/JCLI3321.1.

Stillwell, A. S., C. W. King, M. E. Webber, I. J. Duncan, and A. Hardberger (2011), The Energy-Water Nexus in Texas, *Ecol. Soc.*, *16*(1), 2, doi:10.2139/ssrn.1873566.

Swain, D. L. (2015), A tale of two California droughts: Lessons amidst record warmth and dryness in a region of complex physical and human geography, *Geophys. Res. Lett.*, n/a-n/a, doi:10.1002/2015GL066628.

Tague, C., G. Grant, M. Farrell, J. Choate, and A. Jefferson (2008), Deep groundwater mediates streamflow response to climate warming in the Oregon Cascades, *Clim. Change*, *86*(1–2), 189–210, doi:10.1007/s10584-007-9294-8.

Tanaka, S. K., T. Zhu, J. R. Lund, R. E. Howitt, M. W. Jenkins, M. a. Pulido, M. Tauber, R. S. Ritzema, and I. C. Ferreira (2006), Climate warming and water management adaptation for California, *Clim. Change*, *76*, 361–387, doi:10.1007/s10584-006-9079-5.

Taylor, R. G. et al. (2013), Ground water and climate change, *Nat. Clim. Chang.*, *3*(4), 322–329, doi:10.1038/nclimate1744.

Thomas, B. F., and J. S. Famiglietti (2014), Suistanable Groundwater Management in the Arid Southwestern US: Cochella Valley, california, *Water Resour. Manag.*, *28*, 63–86, doi:10.1016/j.cognition.2008.05.007.

Thyne, G. D. (2004), Hydrologic and geologic factors controlling surface and groundwater chemistry in Indian Wells-Owens Valley area , southeastern California , USA, *J. Hydrol.*, *285*, 177–198, doi:10.1016/j.jhydrol.2003.08.019.

Trenberth, K. E. (2011), Changes in precipitation with climate change, *Clim. Res.*, *47*(1–2), 123–138, doi:10.3354/cr00953.

Velpuri, N. M., G. B. Senay, R. K. Singh, S. Bohms, and J. P. Verdin (2013), A comprehensive evaluation of two MODIS evapotranspiration products over the conterminous United States: Using point and gridded FLUXNET and water balance ET, *Remote Sens. Environ.*, *139*(January), 35–49, doi:10.1016/j.rse.2013.07.013.

Vorosmarty, C. J., P. Green, J. Salisbury, and R. B. Lammers (2000), Global Water Resources: Vulnerability from Climate Change and Population Growth, *Science (80-.).*, *289*(5477), 284–288, doi:10.1126/science.289.5477.284.

Wang, S. Y., L. Hipps, R. R. Gillies, and J. H. Yoon (2014), Probable causes of the abnormal ridge accompanying the 2013-2014 California drought: ENSO precursor and anthropogenic warming footprint, *Geophys. Res. Lett.*, *41*(9), 3220–3226, doi:10.1002/2014GL059748.

Williams, A. P., R. Seager, J. Abatzoglou, B. Cook, J. Smerdon, and E. Cook (2015), Contribution of anthropogenic warming to California drought during 2012 – 2014, *Geophys. Res. Lett.*, 1–10, doi:10.1002/2015GL064924.Received.

Wilson, J. L., and H. Guan (2004), Mountain-Block Hydrology and Mountain-Front Recharge, *Water Sci. Appl. Groundw. Recharg. a Desert Environ. Southwest. United States*, *9*(Plate 1).

Appendix A

PEST output file

```
pcf
* control data
restart estimation
14  3317  4  0  1
3  1  single  point  1  0  0
2.000000e+001  -3.000000e+000  1.000000e-001  1.000000e-001  7 999
lamforgive
1.000000e+001  1.000000e+001  1.000000e-003
1.000000e-001 1 noaui noboundscale
25  3.000000e-001  3  3  1.000000e-002  3
0  0  0   PARSAVEITN
* singular value decomposition
  1
  14  5.000000e-007
  1
* parameter groups
Kx     relative   1.000000e-001  0.000000e+000  switch  2.000000e+000
parabolic
Stor   relative   1.000000e-002  0.000000e+000  switch  2.000000e+000
parabolic
Rech   relative   1.000000e-002  0.000000e+000  switch  2.000000e+000
parabolic
ET     relative   1.000000e-002  0.000000e+000  switch  2.000000e+000
parabolic
* parameter data
Kx2  log  factor  4.837680e-001    1.000000e-002  2.800000e+001    Kx
1.0   0.0 1
Kx3  log  factor  1.149006e+000    1.000000e-002  2.000000e+001    Kx
1.0   0.0 1
Kx4  log  factor  4.316534e-001    1.000000e-002  2.000000e+001    Kx
1.0   0.0 1
ET2  log  factor  1.885216e-002    1.000000e-003  1.000000e+001    ET
1.0   0.0 1
ED2  log  factor  1.136054e+001    1.000000e+000  2.000000e+001    ET
1.0   0.0 1
R2  log  factor  1.000000e-003    1.000000e-003  1.000000e+001    Rech
1.0   0.0 1
R3  log  factor  1.320614e-004    1.000000e-004  1.000000e+001    Rech
1.0   0.0 1
R6  log  factor  4.261568e-004    1.000000e-004  1.000000e+001    Rech
1.0   0.0 1
R8  log  factor  1.000000e-004    1.000000e-004  1.000000e+001    Rech
1.0   0.0 1
R7  none  relative  2.000000e-004    1.000000e-004  1.000000e+001
Rech   1.0   0.0 1
* model command line
pestgv.bat
```

```
* model input/output
lpf.tpl   gv5.lpf
recharge.tpl   gv5.rch
evt.tpl   gv5.evt
targpest.ins   targpest.out
```